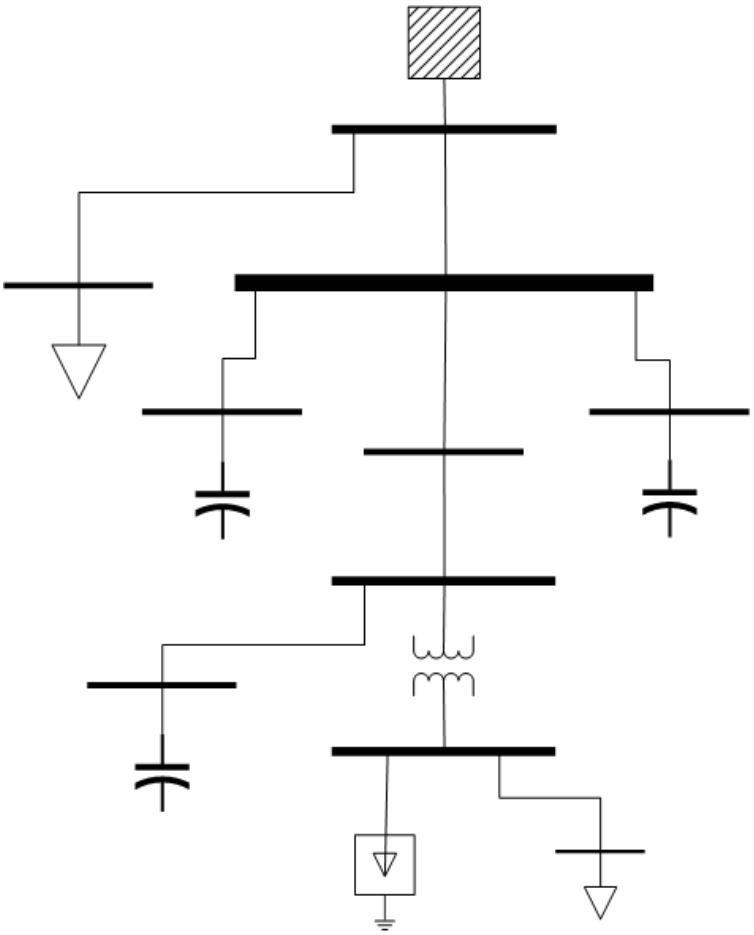

Development of PSS/E Model for Enhanced STATCOM

Master's thesis in Electric Power Engineering

E. Götenfelt, L. Eriksson

DEPARTMENT OF Electrical Engineering
CHALMERS UNIVERSITY OF TECHNOLOGY
Gothenburg, Sweden 2023
www.chalmers.se

Master's thesis 2023

Development of PSS/E Model for Enhanced STATCOM

E. Götenfelt, L. Eriksson

CHALMERS
UNIVERSITY OF TECHNOLOGY

Department of Electrical Engineering
Division of Electric Power Engineering
Chalmers University of Technology
Gothenburg, Sweden 2023

Development of PSS/E Model for Enhanced STATCOM
E. Götenfelt, L. Eriksson

Supervisors: Soubhik Auddy & Ahmed Moawwad, Hitachi Energy
Examiner: Massimo Bongiorno, Department of Electrical Engineering

Master's Thesis 2023
Department of Electrical Engineering
Division of Electric Power Engineering
Chalmers University of Technology
SE-412 96 Gothenburg
Telephone +46 31 772 1000

Typeset in LaTeX
Printed by Chalmers Reproservice
Gothenburg, Sweden 2023

Development of PSS/E Model for Enhanced STATCOM
E. Götenfelt, L. Eriksson
Department of Electrical Engineering
Chalmers University of Technology

Abstract

More and more of the conventional power generation is being replaced by converter-based power generation. This increase of converter-based generation will test the power system with new challenges such as lack of inertia, low network strength and limited fault current injection capability. To address these problems a new Flexible AC Transmission System (FACTS) has been developed, the E-STATCOM, which can provide voltage support in the form of reactive power and frequency support in the form of active power and is a further development of the existing STATCOM. To be able to specify and test that the E-STATCOM is behaving as expected in the connected network, it has to be done multiple studies and analyses. One of the ways that is used to test the product is the power system analysis program PSS®E, which allows for system studies on large networks to be carried out and see how the E-STATCOM behaves during different test cases. In order to carry out these studies in PSS®E a model of the E-STATCOM has to be developed in the programming language FORTRAN. In this project the E-STATCOM is modeled in FORTRAN and tested for its behavior during various cases such as a change in active power load and a change in frequency on the network. The modeled E-STATCOM responds with various results on the tested cases however not fully as desired, a suggestion to a possible solution is made on how to make the E-STATCOM behave fully as intended.

Keywords: FACTS, E-STATCOM, Frequency, Voltage, Stability, PSS®E

Acknowledgements

We would like to thank everyone at Hitachi Energy Västerås that has helped us during our Master thesis. A special thanks to our supervisors Soubhik Auddy and Ahmed Moawwad for your help with the PSS®E and VMPSACD simulations and programming and also for everything we learned from you. Also a special thanks to Afshin Samadi and Pinaki Mitra for giving us the chance to do our thesis with you and for the help with everything. We also want to thank our examinator Massimo Bongiorno for the help with the report writing.

Linus Eriksson & Eric Götenfelt, 2022

List of Acronyms

Below is the list of acronyms that have been used throughout this thesis listed in alphabetical order:

BJT	Bipolar Junction Transistors
CSC	Current Source Converter
E-STATCOM	Enhanced Static Synchronous Compensator
FACTS	Flexible AC Transmission System
FFR	Fast Frequency Response
GFL	Grid Following Control
GFM	Grid Forming Control
GTO	Gate Turn-Off Thyristor
IGBT	Insulated Gate Bipolar Transistor
MOSFET	Metal-Oxide Semiconductor Field-Effect Transistor
MSC	Mechanically Switched Capacitor
MSR	Mechanically Switched Reactor
MSS	External Bank Control
OV	Overvoltage
PLL	Phase-Locked Loop
POD	Power Oscillating Damper
PSC	Power Synchronization Control
RoCoF	Rate of Change of Frequency
SG	Synchronous Generator
STATCOM	Static Synchronous Compensator
SC	Super-Capacitor
UV	Undervoltage
VSM	Virtual Synchronous Machine
VSC	Voltage Source Converter

Contents

1
Introduction

Voltage Source Converter (VSC)-based power generation is becoming increasingly popular in today's power systems such as wind- and solar power generation and it is replacing the conventional generation with a rapid pace. With the increase in penetration of the converter-based generation, the power system is facing new stability challenges, mainly due to lack of inertia, low network strength and limited fault current injection capability of the converters.

To address these problems, new control strategies for the converters are evolving, one such strategy being Grid Forming Control (GFM), where converters act like a voltage source instead of a current source. This strategy enables the converters to be connected to a grid with very low short-circuit level and thus improves the overall stability of the grid. This is possible since the converter with GFM sets its own frequency reference internally and is not affected by the grid's frequency [1]. Comparing this to the grid following control which is more common practice today [2] where the converter synchronizes to the grid frequency and therefore is dependent on a stable grid. As more and more VSC-based power generation is implemented to the grid, the grid following converter will become less and less reliable since there will be less synchronous generators connected to the grid. This will result in a less stable frequency that the grid following converter can synchronize to and will therefore not be a reliable option in the future. Since the GFM-converter is not depending on a stable grid it can be used in weak grids where more converter-based generations are being interconnected.

However, the GFM alone cannot solve the problem of high Rate of Change of Frequency (RoCoF) due to lack of system inertia. It needs an active power source to provide Fast Frequency Response (FFR). The conventional VSC-based devices such as STATCOM are therefore evolving to incorporate energy storage units and turn into Enhanced STATCOMs (E-STATCOM) to fulfill the frequency stability requirements of the grid.

1.1 Aim

The aim of this thesis is to develop a user-defined RMS simulation model of an E-STATCOM with GFM in PSS®E and evaluate the model when compared to a validated VMPSCAD model that Hitachi Energy has available so that the PSS®E model can be used for large-scale system studies.

1.2 Tasks

In this thesis a user-defined RMS simulation model of an E-STATCOM with GFM in PSS®E will be developed and the behavior of the model was originally supposed to be benchmarked with respect to a validated VMPSCAD based E-STATCOM model that is available. An investigation of the possibilities and challenges for representing the DC side dynamics of the energy storage in PSS®E for the E-STATCOM model is to be carried out as well.

To accomplish these tasks the thesis is divided into smaller sub tasks which are:

1. Literature study on related topics such as FACTS (Flexible AC Transmission system), STATCOM, E-STATCOM, GFM and Energy storage.
2. Get familiar with the already existing base STATCOM model in PSS®E.
3. Implement GFM based E-STATCOM model in PSS®E.
4. Validate the model with regards to an existing PSCAD model.
5. Investigate the possibilities and challenges for representing the DC side dynamics of the energy storage in PSS®E for the E-STATCOM model.
6. Implement the DC side dynamics to the model. Control system for the Energy storage and connection to the E-STATCOM.

1.3 Scope

The scope defines what will and will not be included in the thesis. This thesis scope is listed below:

1. The company's ethics and internal guidelines

   The programming code used to run PSS®E will not be shown in the thesis in its entirety because it is Hitachi's model, the code will therefore be kept internally. However this will not have any affect on the thesis' results since the project will focus on the model of the E-STATCOM and the results from PSS®E.
2. PSS®E limitations

   Since the model will be created in PSS®E the thesis is limited to which models and components that can be acquired in PSS®E.

   The programming code for the PSS®E will be written in FORTRAN and Python because FORTRAN is the language used in PSS®E to model components and Python can be used to control the dynamics.
3. VMPSCAD model

   The comparison between PSS®E and VMPSCAD can not be directly compared since the network circuit used for the VMPSCAD-model has two E-STATCOMs. This will make the comparison between the two of them focus more on the general response of the signals in the E-STATCOM and not whether they have a direct match or not.

1.4 Method

The method is split into different tasks and the authors will alternate between working together on some parts and separate on other.

1. Literature study

   The literature study was carried out by reading reports, books and scientific websites regarding relevant information that was necessary in order to get a deeper understanding about the electrical components and systems used in the thesis.

2. Get familiar with the already existing STATCOM model

   This included understanding how the FORTRAN code was constructed and how it was represented by the control systems of the STATCOM and how the FORTRAN language is built up in general. How the Python code was constructed and how to use Python in PSS®E and get a general understanding of how PSS®E is constructed and its applications.

3. Implementation of GFM-based E-STATCOM model in PSS®E

   The company's STATCOM model was developed into an E-STATCOM model in the RMS-based program PSS®E. The authors worked with the model together in the beginning in order for both to be familiar with it. The work was thereafter split up when both authors knew how the model worked.

4. Implement DC side dynamics in PSS®E E-STATCOM model

   This task was foreseen to take the longest time. The DC side (a capacitor) of the existing STATCOM model was as of the start of project represented as a constant DC voltage, this could be done since the capacitor is used to compensate for the active power losses in the converter and they are assumed to be negligible. Since an E-STATCOM was to be modeled an energy storage was added on the DC side to be able to control the injection or consumption of active power to support the grid with frequency stability. For the energy storage to work as expected a control system was implemented.

5. Validate PSS®E E-STATCOM model with E-STATCOM model in PSCAD

   The first part of this task was to understand the E-STATCOM model in PSCAD. The next step was to run the E-STATCOM model in PSS®E and compare it with the already existing E-STATCOM model in PSCAD. The final step was to confirm that the PSS®E E-STATCOM model operates as it was intended to do.

1.5 Format of the report

The report has the following format; First a literature study will be presented with sections that explains the theory behind the E-STATCOM, Super-Capacitor and Grid Forming Control in order to give the reader an introduction to how the different building blocks of this thesis work. Then the already existing STATCOM model will be shown in parts and its control functions will be explained. After that the control parts added for the E-STATCOM will be explained. The results from simulations

for different cases is next. The results will include graphs of different parameters from the E-STATCOM model and text that goes through the graphs. In the next chapter, Discussion, will the behavior of the graphs in the results for the different cases be analyzed and explained. After the discussion comes the conclusion and a section called future work that will explain what could be done next.

2

Literature Study/Theoretical background

This chapter explains the theory regarding power electronic devices and control techniques that are used in this thesis.

2.1 Switching devices

Power electronics is the application of solid-state electrical components that control and convert electric power [3].
FACTS controller is a power electronic-based system that can control one or more parameters in an AC transmission system. Different types of power electronic devices can be connected in parallel or series to achieve the desired characteristic of the controller for its application. The different kinds of power devices used for the controllers can be split into three categories called diodes, transistors and thyristors according to [4] where the diodes are a two-layer family, transistors a three-layer family and thyristors are a four-layer family. The thyristor category can also be called controllable switches according to [5]. An advantage that controllable switches have are the ability to be turned on and turned off by control signals which is useful for FACTS. Some of the controllable switches that are common for FACTS controllers are the Insulated Gate Bipolar Transistor (IGBT) for lower power STATCOMS and Gate Turn-Off Thyristor (GTO) for higher power STATCOM according to [6].

2.1.1 Insulated Gate Bipolar Transistor

The IGBT is a result from experiments to combine Bipolar Junction Transistors (BJT) and Metal-Oxide Semicondutor Field-Effect Transistors (MOSFET) since their characteristics complement each other in areas that are of interest. BJTs have lower conduction losses but rather slow switching and MOSFETs have fast switching but higher losses, combine the two device's advantages and a semiconducting device with relatively fast switching and low losses is created.
The structure of the IGBT is shown in Figure 2.1, at the top of the figure is a metal that is connected to the gate terminal, below that is a layer with an metal oxide, for example silicon oxide, that works as an insulator and below that is the semiconductor region. This structure is called a MOS-structure and its advantages lies in its simple structure and low area requirement.

To turn on the device a positive voltage with respect to the emitter needs to be applied on the gate terminal. When the voltage magnitude is large enough electrons will flow from the n+-region into the p-region. Thus a channel close to the gate will open and allow a current to flow from the collector to the emitter. The device is turned off by removing the applied voltage to close the channel.

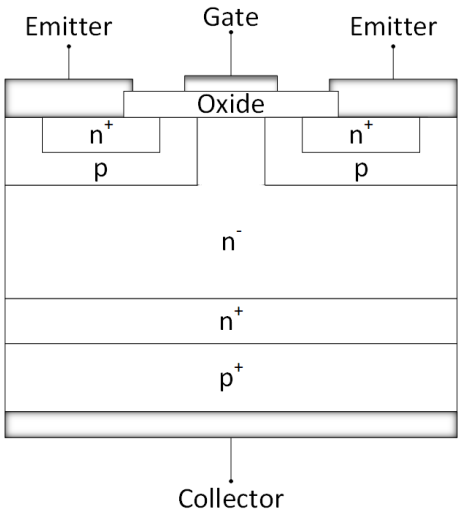

Figure 2.1: IGBT structure.

2.1.2 Gate Turn-Off Thyristor

A GTO can like a conventional thyristor be turned on by a single short-duration current pulse at the gate. Conventional thyrister does not have the ability to turn off the current in the device, instead it can only be turned off when the current in the external circuit goes to zero. This is where the GTO and conventional thyristor differentiates since the GTO can be turned of simply by applying a gate current pulse of the reverse polarity. However the current needed to turn off the GTO is significantly higher than the current needed to turn it on. For example it would require approximately 30 A for a 1000 A device to turn it on but approximately 300 A to turn it off [4].

To go from the thyristor to the GTO some modifications has to be made on the structure and performance of the device. One problem in how the GTO's physics works after some changes is that the carrier lifetime is reduced. However, this can be solved by shortening the anode structure, but this comes with some complications as well. In order for the GTO to turn off, the excess carriers, must be removed by a reverse anode current. But now, due to the shortened anode, this is not possible. So the only way to remove the excess carriers is by internal recombination and diffusion. A convenient part with the structure shown in Figure 2.2 is that the n^+ layer contributes to the rate the excess carriers, holes in this case, gets removed by diffusion in a positive way so that turn-off is possible.

The GTO must usually be used with a snubber circuit since the GTO has a fast current rise time when the device is turned on. The fast rise time is due to the

GTO's interdigitated structure between the gate and the cathode. An interdigitated structure reduces the distances between two electrodes by letting them overlap each other, this is shown in (add figure). Because of this structure overcurrents would flow in the GTO if there are not a turn-on snubber included in the circuit.

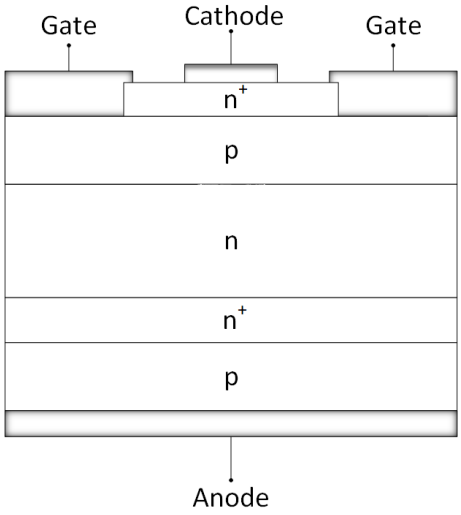

Figure 2.2: GTO structure.

2.2 Voltage Source Converter

The VSC is a conversion device that is used to convert DC to AC or AC to DC, where the direction of the power changes by reversal of the polarity of the DC current whereas the polarity of the DC voltage is always fixed [4]. The technology behind the controller is based on switching devices such as IGBT, which is popular in today's market, or GTO [4]. VSC consists of multiple layers of switching devices in order to control the AC output.

The VSC is preferably used instead of the Current Source Converter (CSC) in FACTS applications for some major beneficial reasons which are:

- The CSCs is in need of power semiconductors with bi-directional voltage blocking capability as in Figure 2.3 and the available semiconductors that can handle the high power levels such as GTOs and IGBTs neither can not block voltages in both directions or will do so on the cost of other important parameters.
- The DC side of the CSC is terminated by a current charged reactor as in Figure 2.3 compared to the VSC which has a voltage charged capacitor as in Figure 2.4, which in turn has much lower losses.
- As can be seen in figure 2.3 the CSC requires a voltage source on the AC side, which in most cases is a capacitive filter that has to be added. The VSC on the other hand requires a current source which is naturally added from the leakage inductance of the coupling transformer.
- The presence of the dc capacitor of the VSC gives a natural protection against voltage transients for the semiconductors, therefore the CSC either needs extra

protection or higher voltage ratings on the semiconductors.
However the current charged reactor of the CSC gives one major advantage over the VSC, with that it is almost entirely immune to terminal shortage due to its current limitation abilities.

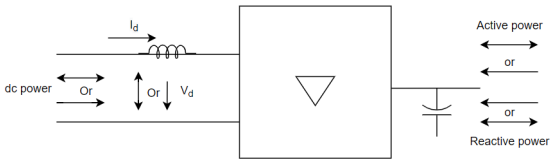

Figure 2.3: Current-source converter.

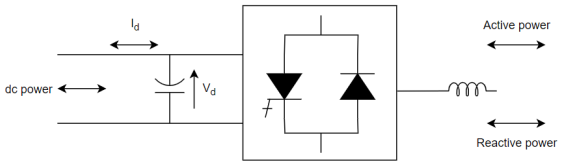

Figure 2.4: Voltage-source converter.

2.3 STATCOM

The way that the STATCOM generates reactive power is on a fundamental level similar to that of a synchronous machine [4]. The schematic of a synchronous machine can be seen in Figure 2.5 and from this it can be seen that the current I can be expressed as (2.1) where V is the system voltage, E is the internal voltage and X is the reactance of the machine plus the leakage reactance of the transformer and the system short circuit reactance. Since there is only reactive power flowing between the grid and the machine, only the magnitude of the voltages has to be taken into account when looking at the equations of the system.

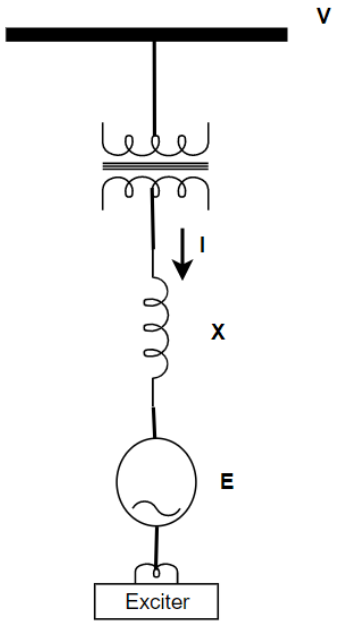

Figure 2.5: Reactive power generation from a synchronous machine.

$$I = \frac{V - E}{X} \tag{2.1}$$

From (2.1) the expression for the reactive power Q can be expressed as (2.2)

$$Q = \frac{1 - \frac{E}{V}}{X} V^2 \tag{2.2}$$

where it can be seen that if the internal voltage E is increased above the grid voltage V (over-excited) there will be a current and also a reactive power flow from the machine to the grid, meaning that it is generating reactive power and if E is decreased below V (under-excited) it is absorbing reactive power. The STATCOM controls the current/reactive power flow in the same way as the machine, where the output voltage of the converter controls whether reactive power is generated or absorbed by the STATCOM. If the converter output voltage is higher than the grid voltage the STATCOM is seen as a capacitor (generates) from the grids perspective and as a reactor (absorbs) if it is lower. The output voltages are generated by a VSC with an energy storage capacitor connected to it, which operates the VSC and the schematic of this can be seen in Figure 2.6. The main function of the DC capacitor is to handle the internal losses of the converter, this needs to be done since the instantaneous power input and output of the converter has to be equal and since there is no active power on the AC side it can not be any active power on the DC side of the converter. There is also an alternative way of handling the internal losses of the converter which is done by lagging the converter voltage by a small angle which will result in the grid supplying the active power for the losses and the DC capacitor can be kept at a desired value. This is beneficial since the output voltage waveform is not a perfect sine wave, due to the reason that it is

generated either by using PWM or by controlling the DC capacitor voltage which is done by controlling the angle of the output voltage, the output voltage will contain ripple. As mentioned before that the instantaneous output and input power has to be equal, if the output voltage contains ripple (current is perfect sine wave) the converter has to draw a ripple current from the DC capacitor (voltage is constant) in order to keep the output and input power equal. So the overall function of the DC capacitor is to keep the instantaneous power input and output of the converter equal.

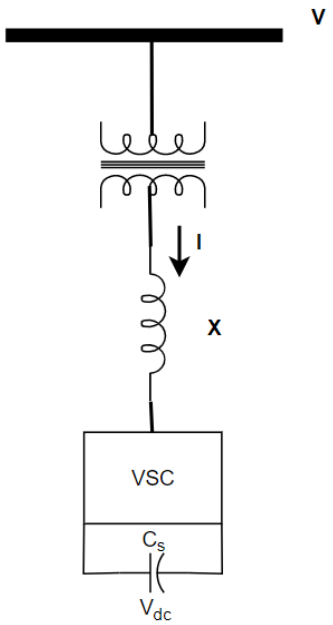

Figure 2.6: Reactive power generation from a STATCOM.

2.4 Super-Capacitor Energy Storage System

The Super-Capacitor (SC) consists of two electrodes and a separator between them that is submerged in electrolyte and allows for ions to travel through but prevents any electrical contact [7]. A representation is shown in Figure 2.7 and it is similar to how a battery usually is constructed.

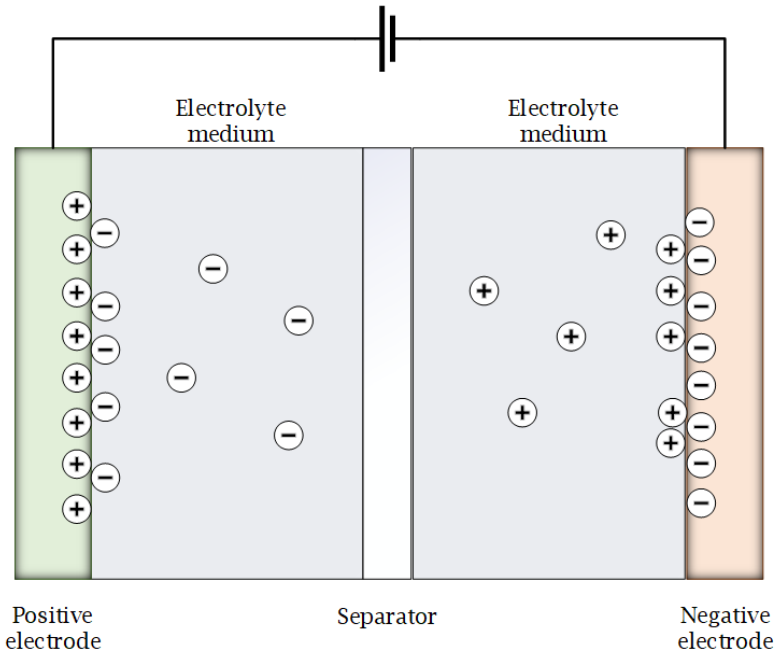

Figure 2.7: Super-Capacitor structure when voltage is applied.

2.4.1 Super-Capacitor vs Traditional capacitor

The difference between a SC and a traditional capacitor, apart from the structure, is that a SC have lower power density, greater charge storage density and different material requirement. This is due to the electrodes' surface area being larger than the ones of a traditional capacitor and because the distance between the charges in the double layer is lower according to [8]. These structure changes results in a higher capacitance according to (2.3)

$$C = \epsilon_r \epsilon_0 \cdot \frac{A}{d} \tag{2.3}$$

where C is the capacitance, ϵ_0 is the permittivity in vacuum, ϵ_r is the relative permittivity of the electrolyte, A is the surface area and d is the distance of the charges. Therefore, by increasing the surface A area and decreasing the distance d the capacitance will have a higher value.

2.4.2 Super-Capacitor Theory

A SC stores energy through the formation of a electric double-layer that occurs at the interface between the electrode and electrolyte once a voltage is applied and the ions begins to move. The theory regarding electric double-layer was first proposed by Hermann von Helmholtz in the 19-century according to [8] where he explains how the ions in the electrolyte approaches the opposite charged electrode to form a layer that balances the total charge and the only thing separating the two charges is the interface of the electrode, this layer is called the Helmholtz layer [9]. Therefore there will be two layers, one of each side of the electrode surface, that results in

a double-layer. The theory was further developed by Gouy, Chapman, Grahame and Stern. Gouy and Chapman added the conditions and effect of ion diffusion and electrostatic forces, which created the Gouy-Chapman layer (Diffuse layer). Then Stern combined the two layers and further developed the Helmholtz layer into two separate layers called the inner and outer plane, this is called the Stern-Grahame model [8]. Figures of the three models can be seen in Appendix A.1. The double-layer can be thought of as a capacitor with two plates of charge that are separated by a distance [10].
The capacitance of an electric double layer can be expressed as

$$\frac{1}{C_{dl}} = \frac{1}{C_H} + \frac{1}{C_d} \tag{2.4}$$

In (2.4), C_{dl} is the capacitance of the double layer, C_H is the capacitance of the Helmholtz layer and C_d is the capacitance of diffuse layer. The equation also indicates that the equivalent circuit of the double layer can be treated as two capacitances in series. Since the Helmholtz layer can be divided into the inner and outer plane according to the Stern-Grahame model, C_H can be expressed as two capacitances in series as well which is shown in (2.5)

$$\frac{1}{C_H} = \frac{1}{C_{IHP}} + \frac{1}{C_{OHP}} = \frac{d_{IHP}}{\epsilon_{IHP}\epsilon_0} + \frac{d_{OHP}}{\epsilon_{OHP}\epsilon_0} \tag{2.5}$$

where C_{IHP} is the capacitance of the inner plane, C_{OHP} is the capacitance of the outer plane, d_{IHP} and d_{OHP} is the distance between the charges, ϵ_{IHP} and ϵ_{OHP} is the relative permittivity of the inner and outer plane. But, the value of ϵ_{IHP} can be relatively low compared to ϵ_{OHP} since the molecules in the inner plane are organised because of the strong electric field while the molecules in the outer plane are distributed more randomly. Therefore the inner planes term will have the most impact when calculating the Helmholtz capacitance. Equation (2.5) can instead be written as

$$C_H = \frac{\epsilon_{IHP} \cdot \epsilon_0}{d_{IHP}} \tag{2.6}$$

The total capacitance of a SC can be split into the capacitance at the positive electrode and the capacitance at the negative electrode and then treat them as series connected. The capacitance at the positive electrode can be expressed as (2.7) and the capacitance at the negative electrode can be expressed as (2.8)

$$C_{dl,p} = \frac{C_{H,p} \cdot C_{d,p}}{C_{H,p} + C_{d,p}} \tag{2.7}$$

$$C_{dl,n} = \frac{C_{H,n} \cdot C_{d,n}}{C_{H,n} + C_{d,n}} \tag{2.8}$$

the total capacitance C_{dl}^T of the SC can be seen as the sum of $C_{dl,p}$ and $C_{dl,n}$ in series and is therefore expressed as

$$C_{dl}^T = \frac{C_{dl,p} \cdot C_{dl,n}}{C_{dl,p} + C_{dl,n}} \tag{2.9}$$

2.4.3 Application

SCs can be used in different areas such as power electronics, computer memory back-up and energy storage. When SCs are used as energy storage system it has some advantages when compared to a battery energy storage system. It is written in [11] that a SC energy storage system has a longer cycle life and high power density but it has a low energy density which is the major shortcoming of the storage system. The life span of a SC is high since it can withstand charges and discharges without having any significant losses in performance. Another advantage the SC has compared to battery according to [12] is its charging efficiency. A lead-acid battery for example can lose up to 30 % of its energy during charging while the SC may only lose 10 %. The major disadvantage with the SC is as mentioned the limited energy density which results in a higher capital cost to maintain the same energy storage level. However, the power density can be 10 times greater than the one of a battery according to [8].

2.5 E-STATCOM

As more and more of the traditional Synchronous Generators (SG) are being phased out such as nuclear power plants and fossil fuel based technologies and replaced by converter based generation, the total inertia of the grid is decreasing. The consequences of this is a weaker system that will have more frequently occurring and severe frequency deviations caused by a mismatch between the generated and absorbed power. By looking at the simple equation of RoCoF (2.10), where df/dt is the RoCoF, f_n is the nominal frequency, ΔP is the mismatch between generated and absorbed power, H is the system inertia constant and S_b is the rated MVA.

$$\frac{df}{dt} = \frac{f_n \Delta P}{2HS_b} \tag{2.10}$$

From this it can be seen that a decrease in H will result in a higher RoCoF, which could lead to loss of synchronism if the frequency changes to fast and the system is not able to recover. The inertia of the SGs allows for the SGs and the grid to be more resistant towards disturbances, in the way that they will slowly decrease or increase their speed and release stored kinetic energy in their turbines/generators, according to [13], in case of a disturbance and give a lower RoCoF and a less severe disturbance. This will give more time for grid operators to take actions against stabilizing the frequency and not losing synchronism. To be able to keep the grid frequency stable also in the future when converter based generation that does not have the same inertia as SGs will be the major part of generation, an upgrade of the STATCOM described above in section 2.3 has been develop called E-STATCOM. The difference is that the E-STATCOM has a large energy storage device (supercapacitor or battery) connected to the DC side of the VSC, which will allow for frequency support by measuring the grid frequency and based on that exchange active power between the grid and the E-STATCOM. Since energy is stored in the energy storage device and it can be controlled to generate active power and therefore supply inertial response when disturbances occur, the grid sees the E-STATCOM as

a SG with inertia, however this type of inertia is refereed to as virtual inertia. GFM is also an important part for this to work since it allows for the E-STATCOM to set/control its own output frequency (not dependent on the the grid frequency) in order to counteract changes on the grid, based on active power measurements and therefore supply the grid with frequency stability.

2.6 Control Theory

Commonly used control functions/filters in the project are here given a short description on how they are built up and the purpose of using them.

2.6.1 Integrator

The integrator is widely used in various control systems [14] and also in this project. It will take an input signal and integrate it over a certain time to get the output. It is built up by an integral in the Laplace domain therefore represented as 1/s and with a time-constant that decides how fast the integrator will respond to its input. Limits can also be added to the integrator, which sets the output to the maximum or minimum limit when it is reached, if desired. An example when it is used is when the voltage across a capacitor has to be calculated over a time span and the current through it is know. The transfer function of the integrator is represented as (2.11), where U(s) is the input, Y(s) is the output and T is the time constant.

$$Y(s) = \frac{1}{sT} \cdot U(s) \tag{2.11}$$

2.6.2 First order Lag-block

The first order lag-block is in this project used to either lag the output signal to represent a physical measurement according to [14], which is done due to the reason that in VMPSCAD when measuring a signal the delay is taken into account and to represent this in PSS®E the lag-block is used. The other reason it is being used is during transients, to allow for a more stable transition between for example a disturbance and steady state, to filter some of the oscillations but at a cost of a longer response time. It consists of a time constant that can be tuned to fit its purpose, the lag-block can also be designed to have limits like the integrator. If desired a gain can be added to control the output signal, if not then it is just set equal to one. The transfer function is according to (2.12).

$$Y(s) = \frac{K}{1 + sT} \cdot U(s) \tag{2.12}$$

2.7 Grid Forming Control

The most used used control system for today's increasing number of converter based generation is Grid Following Control (GFL) and can be modeled as a CSC shown

in Figure 2.3. This control method follows the grids behavior by measuring and synchronizing to the angle of the grid voltage and from that regulates its output power, therefore this method is relying on a stable grid angle/frequency which in today's grid is supplied by the numerous amounts of SGs. The consequence of a decreasing number of SGs is that the grid frequency that the GFL-converters synchronize to will be less and less stable and therefore the GFL control method will not be a viable option in the future. Another control method that is being implemented for converter based generation (mostly in microgrids so far) is the GFM seen in [2] which can be modeled as a VSC as in Figure 2.4. The GFM controls its frequency and voltage output based on measurements of active and reactive power. From the grids perspective the GFM-converter will act in the same way as a SG, however since it is converter based it can change its frequency and voltage output almost instantaneously, and therefore being able to handle frequency and voltage deviations much faster than the SG and avoid potential load shedding.

There are two major control systems used for the control of the GFM-converter. These are droop control, according to [15], and virtual synchronous machine (VSM) control. The droop control is based on two linear equations (2.13) and (2.14)

$$\omega = \omega^* - m \cdot P \tag{2.13}$$

$$V = V^* - n \cdot Q \tag{2.14}$$

where ω and V are the converter output angle frequency and voltage amplitude, ω^* and v^* are the reference values, P and Q are the changes in active and reactive power from the set point and m and n are droop coefficients as (2.15) and (2.16)

$$m = \frac{\Delta\omega}{P_{max}} \tag{2.15}$$

$$n = \frac{\Delta V}{Q_{max}} \tag{2.16}$$

where $\Delta\omega$ and ΔV are the maximum angle frequency and voltage amplitude deviations the converter can handle and P_{max} and Q_{max} are the maximum output powers of the converter.

The working principle is understood by looking at the above equations and Figure 2.8, where if there is a change in the load the angle frequency changes to a higher or lower value to compensate and allow for the output power of the converter to change accordingly. The angle frequency is then restored to the nominal value by changing the reference value and therefore moving the linear function in Figure 2.8 up or down and still supplying the same load. In practice the angular frequency control can be replaced by frequency control, but the same principal applies. The same procedure is also applied for the voltage-reactive power droop control.

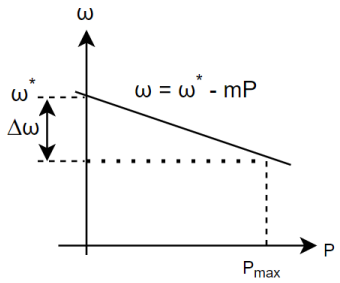

Figure 2.8: Working principal of droop control.

However for the droop control to work as intended a virtual inductive impedance has to be implemented, for the reason that droop controllers were designed for lines with a major inductive part [16]. In smaller grids where the lines are shorter the resistive part of the line impedance will cause large variations on the converter outputs, making it harder to match the voltage and reactive power between sources [16].
The other part that is used to control the GFM-converter is the VSM control which is based on the swing equation of a synchronous machine which are (2.17) and (2.18)

$$M\frac{d\omega_r}{dt} = P_e - P_m \tag{2.17}$$

$$\frac{d\theta_r}{dt} = \omega_r \tag{2.18}$$

where M is the moment of inertia, ω_r is the rotational speed of the rotor, P_e is the electrical power, P_m is the mechanical input power and θ_r is the rotor angle. The only difference when applying the swing equation to the GFM-converter is that P_m is replaced with P_{ref}.
Its principle is called Power Synchronization Control (PSC) and as the name suggests it uses the measured active power to set the output frequency of the converter and synchronize to the grid. The diagram of the control system can be seen in Figure 2.9 where the upper part is the PSC and the lower is the phase-locked loop (PLL) which is the method that is being used by GFL to synchronize to the grid. The PLL is used as a complementary to the PSC. Where P_{ref} is set according to if the E-STATCOM needs to contribute with frequency support in the form of active power contribution and is set according to (2.19)

$$P_{ref} = P^0_{ref} + K_g(\omega_r - \omega_1) + K_f(\omega_r - \omega_f) \tag{2.19}$$

where P^0_{ref} is the nominal power reference, the second term is a droop term with droop coefficient K_g and ω_1 is the reference frequency. The third term is a damping term with damping gain of K_f and ω_f is a low-pass filtered ω_r. So if there is an increase in ω_r, P_{ref} will increase which in turn will lower the value on the right hand side of (2.17) and that will cause a decrease in the RoCoF (left hand side of (2.17)) to stabilize the system.

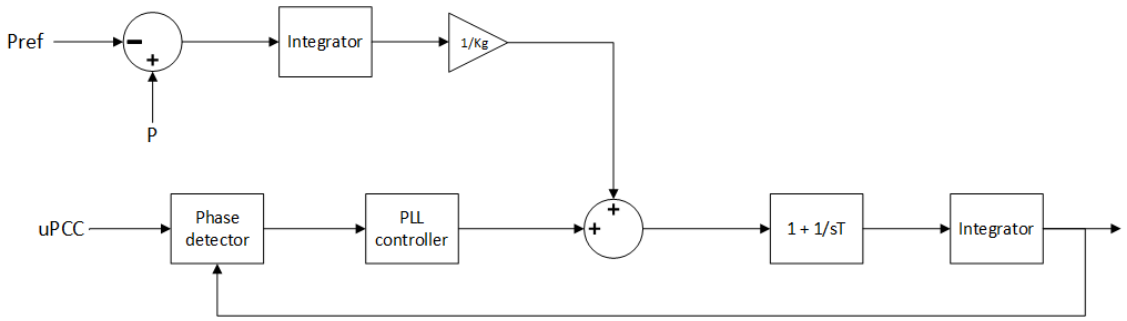

Figure 2.9: PSC and PLL implementation for GFM synchronization.

The time constant of the integrator in Figure 2.9 represents the inertia of the PSC and can be set as desired, K_G sets the proportional gain of the PSC. For a STATCOM the time constant is set very low since there is no energy storage unit that can provide the virtual inertia to the system, so the time constant more or less only applies for an E-STATCOM.

2.8 Clarke and Park transformation

The Clarke and Park transformations are used to simplify the calculations when dealing with a three-phase AC machine because the mathematical equations can be complex since variables such as flux linkages, induced voltages and currents are all time varying. Therefore it is easier to do the calculations by first transforming these quantities from a three-phase AC behavior to a two-phase DC behavior. The vector representation of the transformations and the three-phase reference frame are shown in Figure 2.10.

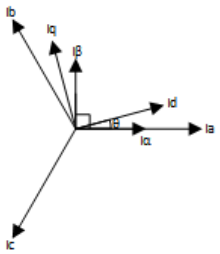

Figure 2.10: Vector representation of Clarke and Park transformation.

2.8.1 Clarke Transformation

The Clarke transformation converts a three-phase quantity from a three-phase reference frame to a two-phase stationary reference frame where the the two phases, α and β, are orthogonal to each other. The transformation can be derived from a three-phase system that is symmetric and balanced, where the three phases is described as

$$I_a = \hat{I} sin(\omega t + \theta) \tag{2.20}$$

$$I_b = \hat{I}sin(\omega t + \theta + \frac{2\pi}{3}) \tag{2.21}$$

$$I_c = \hat{I}sin(\omega t + \theta - \frac{2\pi}{3}) \tag{2.22}$$

By assuming that the A-axis is aligned with the α-axis as in Figure 2.10 the current in $\alpha\beta$-frame can be calculated with the following equations

$$I_\alpha = I_a cos(0) + I_b cos(\frac{2\pi}{3}) + I_c cos(-\frac{2\pi}{3}) = I_a - \frac{1}{2}I_b - \frac{1}{2}I_c \tag{2.23}$$

$$I_\beta = I_a sin(0) + I_b sin(\frac{2\pi}{3}) + I_c sin(-\frac{2\pi}{3}) = \frac{\sqrt{3}}{2}I_b - \frac{\sqrt{3}}{2}I_c \tag{2.24}$$

The transformation can be expressed mathematically by a matrix as shown in (2.25)

$$\begin{bmatrix} I_\alpha \\ I_\beta \end{bmatrix} = K \begin{bmatrix} 1 & -\frac{1}{2} & -\frac{1}{2} \\ 0 & \frac{\sqrt{3}}{2} & -\frac{\sqrt{3}}{2} \end{bmatrix} \begin{bmatrix} I_a \\ I_b \\ I_c \end{bmatrix} \tag{2.25}$$

where I_a, I_b and I_c are currents in the three-phase frame. I_α and I_β are currents in the stationary two-phase frame and K is the scale factor. The scale factor K is a constant that can be set to a specific value depending on if the system should be power invariant or amplitude invariant. For a power invariant system K is set to $\frac{\sqrt{2}}{3}$ and for an amplitude invariant system K is set to $\frac{2}{3}$.

2.8.2 Park transformation

The Park transformation is used to convert the two-phase stationary reference frame from the Clarke transformation to a two-phase rotating reference frame where the two components are called d and q. Just like α and β the vectors are orthogonal. The equations for the Park transformation are shown in (2.26).

$$\begin{bmatrix} I_d \\ I_q \end{bmatrix} = \begin{bmatrix} cos(\theta) & sin(\theta) \\ -sin(\theta) & cos(\theta) \end{bmatrix} \begin{bmatrix} I_\alpha \\ I_\beta \end{bmatrix} \tag{2.26}$$

where I_d and I_q are the quantities in rotating reference frame and θ is the rotation angle.

2.8.3 Machine Reference Frame

With the help of Clarke and Park transformations the d and q component can be used for a machine with the d-axis aligned with the rotor flux and the q-axis with the back EMF of the stator. This can be shown by a stator model in steady state shown in Figure 2.11.

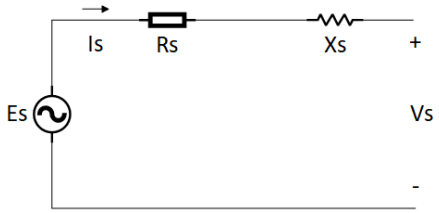

Figure 2.11: Stator model in steady state.

Figure 2.11 can be derived into (2.27) shown below

$$E_s = (R_s + jX_s)I_s + V_s \tag{2.27}$$

Where E_s is the back EMF, R_s is the stator resistance, X_s the stator reactance, I_s stator current and V_s the terminal voltage. The back EMF can be calculated by computing the derivative of the field winding flux according to Faraday's law of induction(add source), shown in (2.28)

$$E_s = \frac{d\Psi_m}{dt} \tag{2.28}$$

where Ψ_m is the field winding flux. Now lets introduce the dq-components and choose to align the d-axis with the flux. The flux can be expressed as in (2.29)

$$\Psi_m = \hat{\Psi}_m \cdot sin(\omega t) \tag{2.29}$$

where ω is the angular frequency. With this equation the back EMF can be calculated with the following formula

$$E_s = \frac{d\Psi_m}{dt} = \omega\hat{\Psi}_m \cdot cos(\omega t) \tag{2.30}$$

By comparing (2.29) and (2.30) it can be seen that the flux is expressed as a sine wave and the back EMF as a cosine wave which results in a 90 degree phase shift between the two quantities. Now lets introduce the dq-components and choose to align the d-axis with the flux. Since the back EMF leads the flux by 90 degrees and the d and q component is separated with 90 degrees, the q-axis will align with the back EMF. The vector representation is shown in Figure 2.12

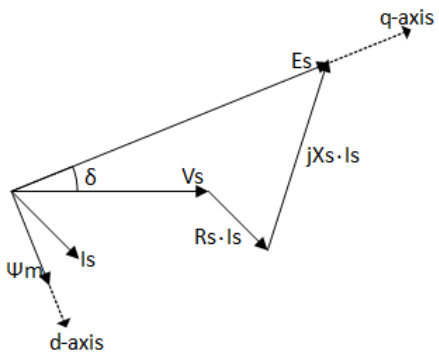

Figure 2.12: Vector representation of stator model in steady state

2.8.4 Grid Voltage Reference Frame

For a simple two-bus system that is built up just like the stator model in Figure 2.11 the dq-components can be used to simplify calculations, this is called Grid Voltage Reference Frame. The difference from Machine Reference Frame and Grid Voltage Reference Frame is where the d and q-axis is aligned. For a power system the d-axis aligned with the grid voltage V_s since that results in the grid voltage to only have a d-component and no q-component because its value is 0. Why this is convenient can be explained by looking at the calculated apparent power in the system shown in (2.31) and (2.32)

$$S_s = V_{s,dq} \cdot I^*_{s,dq} = (V_{sd} + jV_{sq}) \cdot (I_{sd} - jI_{sd}) \tag{2.31}$$

$$S_s = P_s + jQ_s \tag{2.32}$$

where S_s is the apparent power. By combining (2.31) and (2.32) the real and imaginary part can be calculated which results in the following equation

$$P_s + jQ_s = (V_{sd} \cdot I_{sd} + V_{sq} \cdot I_{sd}) + j(-V_{sd} \cdot I_{sq} - V_{sq} \cdot I_{sd}) \tag{2.33}$$

Since the q-component of the grid voltage is 0. Equation (2.33) can be simplified into (2.34)

$$P_s + jQ_s = V_{sd} \cdot I_{sd} + j(-V_{sd} \cdot I_{sq}) \tag{2.34}$$

This gives the following formulas for the active and reactive power in dq-coordinates

$$P_s = V_{sd} \cdot I_{sd} \tag{2.35}$$

$$Q_s = -V_{sd} \cdot I_{sq} \tag{2.36}$$

where I_{sd} can be called the active current and I_{sq} the reactive current.
The vector representation for the Grid Voltage Reference Frame is shown in Figure 2.13.

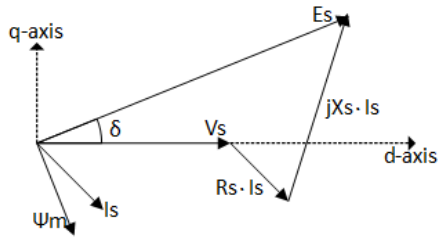

Figure 2.13: Stator model in steady state.

3

E-STATCOM model

3.1 Existing STATCOM model

This project is based on an already existing STATCOM model with GFM-control. This means that most of the basic functions needed for the E-STATCOM model with GFM-control was implemented in the existing model, such as limiters (current, reactive power and secondary voltage) for the output of the E-STATCOM, PI-regulator to control the current based on voltage variations, under- and over-voltage strategies and various functions to set the reference value of the voltage which is to be compared with the actual bus voltage. Since some of the parts in this project is a further development of the already existing model a description of the existing base functions has to be made in order to understand the implementations that has been done during this project.

3.1.1 Automatic Voltage Regulator

The automatic voltage regulator is the core of the model and can be seen in Figure 3.1. It sums up four different voltage signals into one signal that is the reference signal of the voltage, which contains V_{ref},SV_{ref}, V_{podL} and V_{slope}. Where V_{ref} is set internally in the STATCOM to a desired value and can be seen as the main reference voltage. SV_{ref}, V_{podL} and V_{slope} are used to correct the final reference signal and will be described later. After these signals are summed up they pass through a limiter which limits the signal between V_{min1} and V_{max1}. By comparing the output signal from the limiter with V_{resp} which is the voltage on the regulated bus V_{bus}, but with a delay representing the voltage measurement, the error V_{err} is created and used as an input to the PI-regulator. The regulator outputs I_{vsc} based on the proportional gain K_{pv} and integral gain K_{iv}, the regulator also has a upper limit I_{vsc_max} and lower limit I_{vsc_min} in order to limit the output signal.

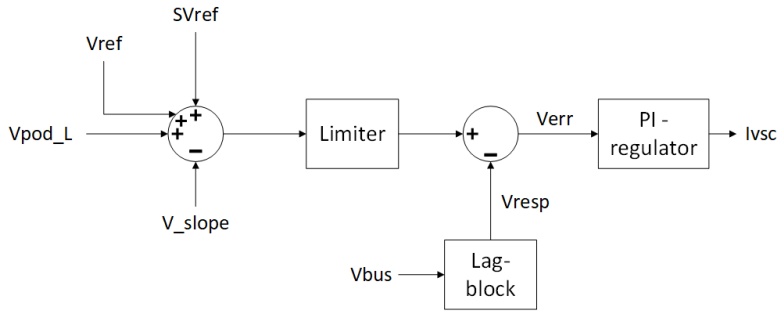

Figure 3.1: Automatic voltage regulator.

3.1.2 Slow MVAR Control

The slow MVAr function is contributing SV_{ref} to the reference voltage and its block diagram can be seen in Figure 3.2. It has one part for capacitive operation which is the upper half of the block diagram with V_{REFMAX} and Q_{REGMAX} and one for inductive operation with V_{REFMIN} and Q_{REGMIN}. The slow MVAr will bring the voltage at point of common coupling (PCC) slowly below V_{REFMAX} in capacitive operation and above V_{REFMIN} in inductive operation. This will allow for the STATCOM to have some spare MVAr in case of emergency operation. For the capacitive region Q_{prim} (STATCOM output MVAr) is compared to Q_{REGMAX} and passed through a limiter according to Figure 3.2 and then through an integrator which output SV_{ref}. The output signal will either decrease or increase the reference voltage depending if it is operating in capacitive or inductive region. Since this function is slow compared to the PI-regulator described above, the integrator's time constant is large to allow for a slow change in the reference value.

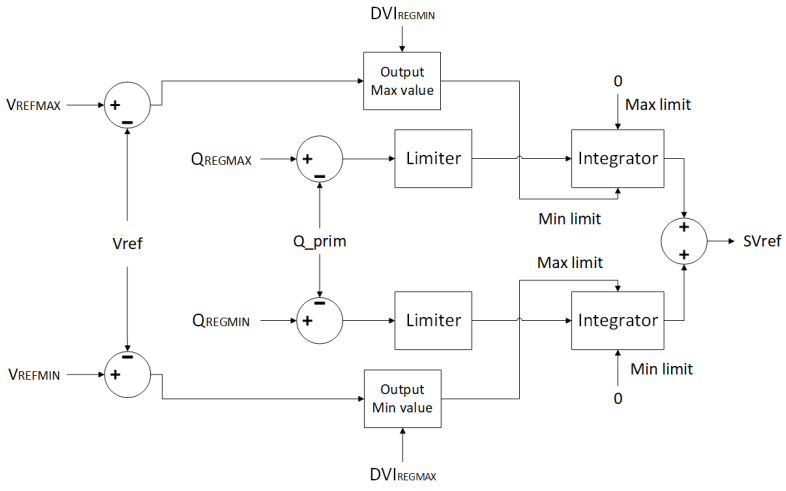

Figure 3.2: Block diagram of Slow MVAr control.

3.1.3 POD

The power oscillating damper (POD) is a function that dampens the active power oscillations in the q-component in the system and the block diagram can be seen

in Figure 3.3. This is done by contributing with V_{podL} to the reference voltage in Figure 3.1. It takes either the active power or the frequency deviation as input and pass it through a number of lead-lag and washout filters in order to filter out the oscillations. The output from these filters are then limited by U_{lim} and L_{lim} in order to get V_{podL}. These limits are set by multiplying V_{PODMAX} and V_{PODMIN} with a ramp function in order to not use the entire region of V_{PODMAX} and V_{PODMIN} but instead gradually increase the limits and the output. Figure 3.4 shows the flow chart of the ramp function used to deactivate the POD by setting the ramprate to a large negative value which will set the ramp and the limits to zero. This is needed in the case when either over- or under-voltage strategies are active since that will create a conflict between them.

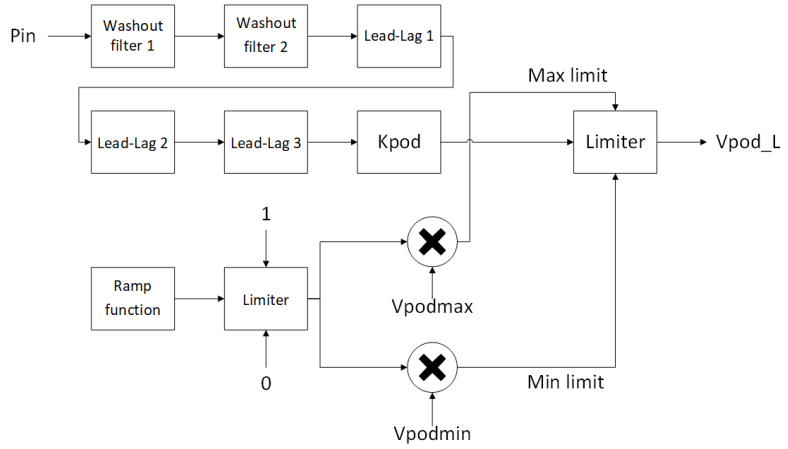

Figure 3.3: Block diagram of Power oscillation damper (POD).

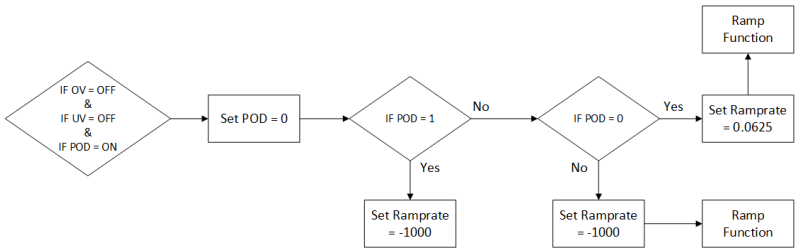

Figure 3.4: Flow chart of the Ramp function.

3.1.4 Slope (droop) control

The droop control is a gain block that multiplies the final output of the STATCOM I_{out_q} with an inductive or capacitive reactance (depending on capacitive or inductive operation) and outputs V_{slope} seen in Figure 3.5. V_{slope} is then subtracted in Figure 3.1 to control the voltage reference.

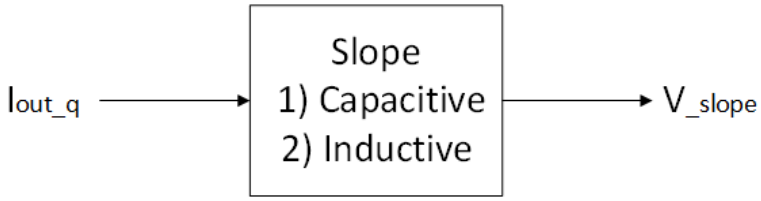

Figure 3.5: Block diagram Slope (droop) control.

3.1.5 Gain Supervisor and Optimizer

The gain supervisor is used to supervise the output of the PI-regulator and regulate the integral gain K_{iv} if the output I_{VSC} is oscillating. This is done by steps of 5% each time step until the peak-to-peak value of I_{VSC} is at a desired value. The gain optimizer also supervises the output but it sets K_{iv} back to its original value when the gain supervisor is done regulating it and the current is stabilized. The block diagram of the gain supervisor and optimizer can be seen in Figure 3.6.

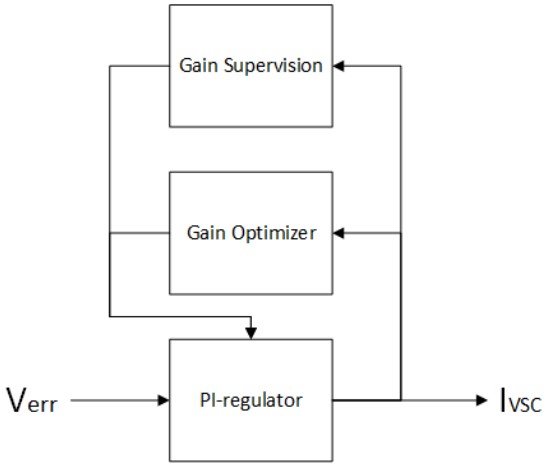

Figure 3.6: Block diagram Gain supervisor and optimizer.

3.1.6 External Bank Control (MSS)

Depending on the STATCOM's output current the External Bank Control (MSS) can switch in or switch out Mechanically Switched Capacitors (MSC) or Mechanically Switched Reactors (MSR), also known as shunt capacitor/reactor banks. The reason for using external shunt banks is that it helps the STATCOM during extreme conditions. MSC provides grid stabilization and voltage control during heavy load conditions and MSR provides stabilization under low load conditions [17].

In the STATCOM model there are two switching methods applicable for both MSC and MSR, a slow switching method and a fast switching method. The slow switching is the most commonly used method of the two while fast switching is used only if necessary. There are three parameters used in each of the methods, two current values that indicates when the MSS should switch and a time delay that shows how long a condition must hold for the MSS to switch. MSS will be switched in if the output current I_{VSC3} has a higher value than I_{High}^{slow} for a time of T_{Delay}^{slow} and will be

switched off if the output current I_{VSC3} has a lower value than I_{High}^{slow} for a time of T_{Delay}^{slow}. The logic behind the fast switching method is same and the relationship between the parameters are shown below:

$$I_{Low}^{fast} < I_{Low}^{slow} < I_{High}^{slow} < I_{High}^{fast} \tag{3.1}$$

$$T_{Delay}^{fast} < T_{Delay}^{slow} \tag{3.2}$$

To prevent rapid switching between the two methods and that they does not get switched in at the same time, a switching delay is implemented.

3.1.7 Limiters

The limiters are used to keep the output current, reactive power and STATCOM bus voltage within set limits. These set limits are defined by the user and tuned depending on what equipment that is used inside of the STATCOM, for example the IGBTs can only withstand a certain amount of current and therefore the limits have to be set according to that amount or to any other component that is more sensitive. If there is a signal that exceeds its limit during a set amount of time the limiters will reduce the output current of the STATCOM.

As can be seen in Figure 3.8 and 3.9 there are five limiters that covers both capacitive (positive) and inductive (negative) operation. In capacitive operation the voltage at the secondary side of the transformer (between the STATCOM and the bus connecting it to the grid), the current and the reactive power is limited and in inductive operation the current and reactive power is limited. The capacitive limiters controls the maximum output of the PI-regulator I_{vsc_max}, by taking the minimum output of the three limiters and setting I_{vsc_max} to that value and thereby overwriting the default setting of I_{vsc_max} and decreasing the output current. The inductive limiters controls the minimum output of the PI-regulator I_{vsc_min} in the same way as the capacitive, but instead of the minimum output it takes the maximum output of the limiters, seen in Figure 3.7. The different limiters are as following:

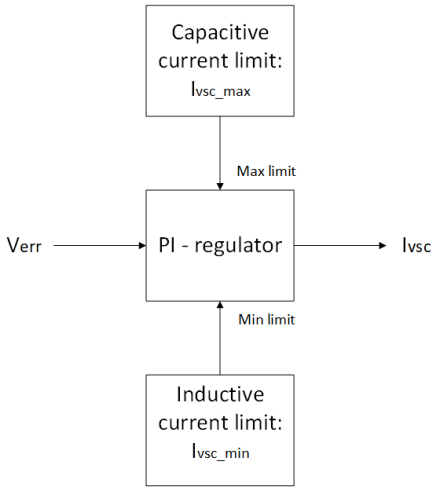

Figure 3.7: Block diagram of capacitive and inductive limiters.

Secondary Voltage Limiter: It monitors the voltage at the secondary side of the transformer V_{2LV} and passes it through a lag block with time constant T_6 which represents a delay in voltage measurement. The voltage is then compared to V_{2MAX} and the error is then checked if it goes below zero for a longer period than T_{ON1} and if that is the case the error is passed to the integrator with time constant T_7, where T_7 controls the speed of the integrator which in turn controls the speed of the limiter.

Capacitive Current Limiter: It monitors the current between the secondary side of the transformer and the STATCOM I_{1HV} and passes it through a lag block with time constant T_8 which represents a delay in current measurement. The current is then compared to I_{1MAXC} and the error is then checked if it goes below zero for a longer period than T_{ON2} and if that is the case the error is passed to the integrator with time constant T_9, where T_9 controls the speed of the integrator which in turn controls the speed of the limiter.

Capacitive Reactive Power Limiter: It monitors the reactive power between the secondary side of the transformer and the STATCOM Q_{Prim} and passes it through a lag block with time constant T_{16} which represents a delay in measurement. The reactive power is then compared to Q_{1MAXC} and the error is then checked if it goes below zero for a longer period than T_{ON3} and if that is the case the error is passed to the integrator with time constant T_{14}, where T_{14} controls the speed of the integrator which in turn controls the speed of the limiter.

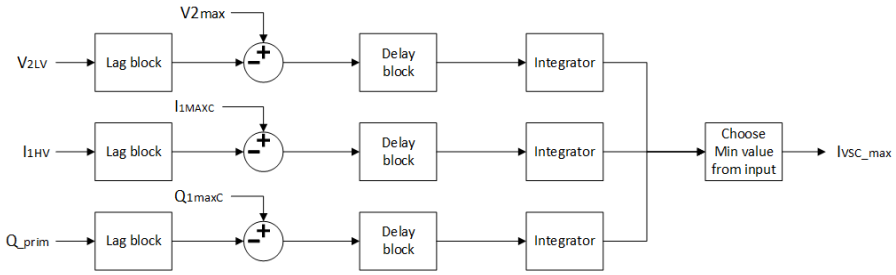

Figure 3.8: Block diagram of capacitive limiters.

Inductive Reactive Power Limiter: It monitors the reactive power between the secondary side of the transformer and the STATCOM Q_{Prim} as well and passes it through a lag block with time constant T_{17} which represents a delay in measurement. The reactive power is then compared to Q_{1MINI} and the error is then checked if it goes above zero for a longer period than T_{ON5} and if that is the case the error is passed to the integrator with time constant T_{15}, where T_{15} controls the speed of the integrator which in turn controls the speed of the limiter.

Inductive Current Limiter: It monitors the current between the secondary side of the transformer and the STATCOM I_{1HV} as well and passes it through a lag block with time constant T_{10} which represents a delay in current measurement. The current is then compared to I_{1MINI} and the error is then checked if it goes above zero for a longer period than T_{ON4} and if that is the case the error is passed to the integrator with time constant T_{11}, where T_{11} controls the speed of the integrator which in turn controls the speed of the limiter.

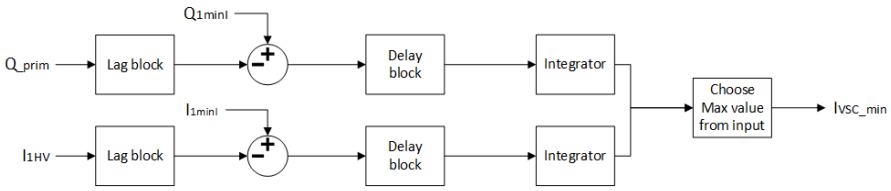

Figure 3.9: Block diagram of inductive limiters.

3.1.8 Undervoltage and Overvoltage Strategy

Overvoltage (OV) and Undervoltage (UV) are mainly used to protect the STATCOM and network. UV and OV has the voltage V_{bus} at a chosen bus as input and if the voltage limit is violated the STATCOM voltage from the PI-regulator will be switched to a constant value specified by the user.

3.1.9 Overvoltage

The OV strategy has two different voltage levels, $OV_{threshold}$ and OV_{trip} where OV_{trip} has a higher value than $OV_{threshold}$. If V_{bus} has a value between $OV_{threshold}$ and OV_{trip} the STATCOM will output maximum inductive current to counteract the voltage. If V_{bus} continues to have a voltage between $OV_{threshold}$ and OV_{trip} for a specified time declared as $T_{OV\,Block}$ the OV strategy will block the output current instead. This is done to protect the equipment from damage and eventually breaking. If the voltage problem is present still after a specified time declared as $T_{OV\,Trip}$, the STATCOM will trip.

3.1.10 Undervoltage

The UV strategy is usually applied during severe undervoltage caused by a fault. If a fault occurs the STATCOM will initially try to bring back the voltage to V_{ref} by applying maximum capacitive current until UV strategy is applied. Similar to the OV strategy there are two voltage levels specified in the UV strategy as well, called UV_{1Low} and UV_{2Low}. The UV strategy will start if V_{bus} has a value between UV_{2Low} and UV_{1Low} where $[UV_{2Low}<UV_{1Low}]$. If this conditions is reached the STATCOM output current will be set to a specified value that is close to zero in order to avert a voltage overshoot when the fault is cleared. If V_{bus} drops below UV_{2Low}, the output current will be blocked to protect and will continue to be blocked until V_{bus} has a higher value than UV_{1Low}.

3.1.11 Grid forming control (GFM)

The grid-forming control is introduced to handle higher RoCoF when there is less inertia in the system with instant frequency support. It also supplies the E-STATCOM with the parameters needed to internally set its voltage magnitude and angle and therefore not depend on a stable grid voltage. The GFM-control scheme is implemented after the voltage regulator seen in Figure 3.1 where previously it was only passed through a lag-block and scaled to the system base and then injected to the

system. Where now when the GFM is introduced the block diagram looks like in Figure 3.10.

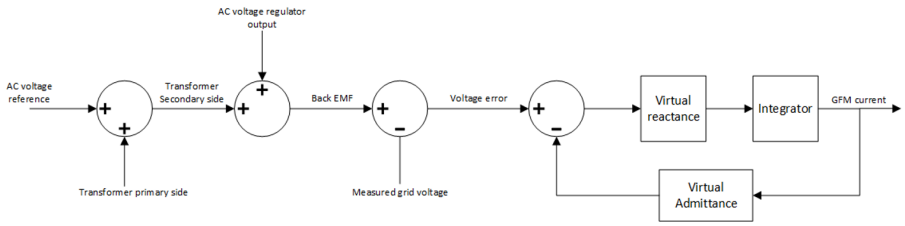

Figure 3.10: Block diagram of Grid Forming Control.

The virtual impedance represents an impedance introduced between the E-STATCOM and the load which allows for a change in the effective impedance [18]. This is highly needed for weak grids which have a high source impedance and undergo large variations, the virtual impedance can control the impedance of the E-STATCOM to match the impedance of the grid allowing it to react to the bigger changes that occurs in a weak grid. This means that the virtual impedance is unique and tuned to fit the grid it is connected to.

The equations that are formed to get the GFM-current is first the voltage drop across the virtual impedance (3.3) where E_{EMF} is the back EMF and U_{sec} is the measured voltage at the secondary side of the transformer (E-STATCOM side).

$$U_{err} = E_{EMF} - U_{sec} \tag{3.3}$$

E_{EMF} (3.4) consists of two parts, the AC voltage reference (adjusted to the secondary side) where X_T is the transformer impedance and the contribution from the voltage regulator described above I_{VSC}, multiplied with the virtual impedance.

$$E_{EMF} = (U_{ref\_prim} + I_{prim} \cdot X_T) + I_{VSC} \cdot Z_{virt} \tag{3.4}$$

Then the GFM-current I_{GFM} is formed according to (3.5) in the Laplace domain,

$$I_{GFM} = \frac{1}{sT_{GFM}} \cdot \frac{U_{err} + I_{GFM} \cdot Z_{virt}}{L_{virt}} \tag{3.5}$$

where T_{GFM} is the time constant, which is tuned to fit the according network, I_{GFM} is the looped back value of the GFM-current and L_{virt} is the virtual inductance which is added to increase the stability of the system [19]. This GFM-current is then used as the injection current into the system and used for the next iteration in solving the system. Equation (3.5) is derived from a simple system where a VSC is connected to an AC system through a resistor and inductance [20].

3.2 Modeling and Control of DC System as the Energy Storage

The control system of the energy storage is built up in several steps. First of all how to represent the DC-voltage, then the connection between the DC-voltage and the *d*-*q* transformations of the network voltages and currents. Then the synchronization to the grid and lastly the representation of the final current in *d*- and *q*-coordinates that will be injected to the network.

3.2.1 Representation of DC-voltage

In order to be able to control the DC-side energy storage, an investigation had to be done to find out how the GFM-current is linked to the DC-voltage across the super-capacitor (energy storage). This investigation was done by looking at how the existing E-STATCOM model in VMPSCAD and Hi-Draw is linking the DC-voltage and GFM-current reference. First simulations of a frequency change were performed in VMPSCAD to find out how the super-capacitor is charged/discharged during a frequency change (looking at how the voltage over the super-capacitor changes) and then compare that to i_{d_vsc} which is the d-component of the current output from the E-STATCOM and the current going through the super-capacitor. This in order to see if they have a similar dynamic/behavior, this was noticed and can be seen in Figure 3.11 and based on this the link between the GFM-current and the DC voltage, it was further looked into in Hi-Draw.

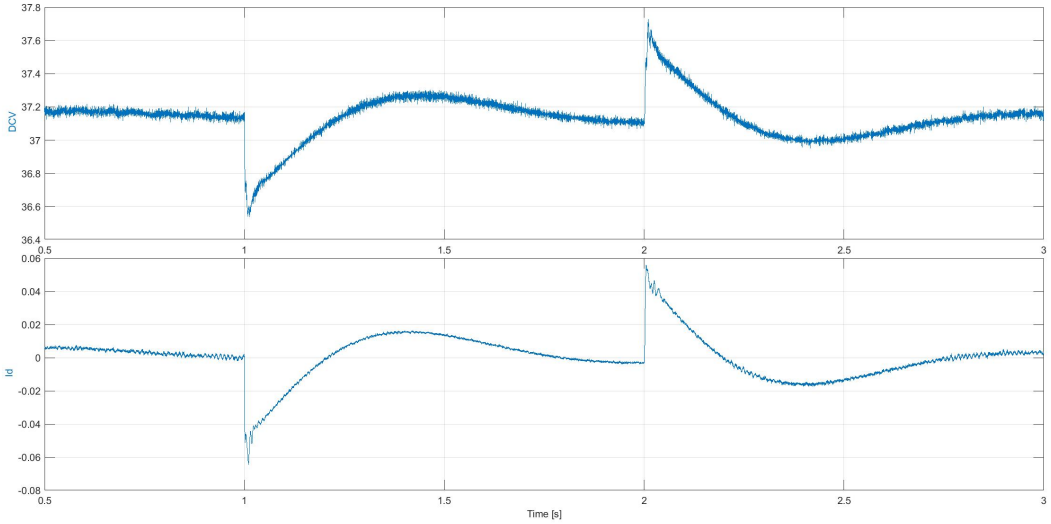

Figure 3.11: Comparison between the DC-voltage across the super-capacitor and the d-component of the current.

Hi-Draw is the program that is used to build up the internal control signals that are being used in the VMSPCAD model, here one can trace back the signals that are used to finally create the GFM-current and possibly find a link that goes back to the

DC voltage. It was found that one of the signals that are used to create the GFM-current is the DCREG_KP, which is the current reference from the contribution from the DC-voltage and is calculated according to Figure 3.12 and this parameter can also be represented in the PSS®E-model.

This investigation has to be done since PSS®E is an RMS-based program and it is not designed to measure or simulate DC voltages, that means that the DC voltage has to be calculated based on the measurements that are available in PSS®E. Looking at the block diagram in Figure 3.12 it is noted that the input to the calculation is P_{OUT} which can be measured in PSS®E by measuring the active power out of the E-STATCOM bus. In order to calculate the DC-voltage it is looped back and P_{OUT} is divided by it in order to get the DC-current. Then by dividing the DC-current with the constant C_{DC} which is the equivalent DC capacitance in pu of one phase leg in the converter and then integrating that signal the DC-voltage is calculated. Then as mentioned before it is looped back with the updated value. By looking at the transfer function (3.6) of the integrator (Y(s) is output and U(s) is input) and comparing with the equation for the voltage across a capacitance (3.7) it is noted that the time constant in the transfer function is equivalent to the cell capacitance. Therefore the time constant can be replaced with the value of C_{DC} and then the division by C_{DC} can be removed and instead included in the integrator. This time constant was tuned to fit the network it was connected to.

$$Y(S) = \frac{1}{sT} \cdot U(S) \tag{3.6}$$

$$V_{DC} = \frac{1}{C_{DC}} \int i_{DC} dt \tag{3.7}$$

After the DC-voltage has been calculated it is divided by the voltage base U_{DC_BASE} to convert it to pu and then it is compared to the DC-voltage reference value V_{DC_ref} to get the error. The error is then multiplied with a gain in order to end up with the DC-voltage contribution current reference DCREG_KP which as mentioned represents how much the DC-voltage is changed and that will affect the GFM-current and the Power Synchronization Control (PSC).

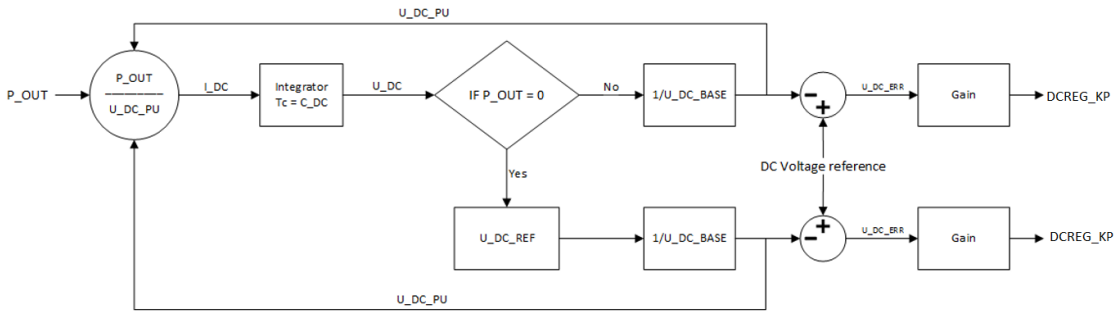

Figure 3.12: Calculation of current reference based on DC-voltage contribution based on active power measurement.

3.2.2 d- and q-component for GFM

With the contribution from the energy storage/DC side defined the equations for the d- and q-component of the GFM-current can be fully expressed. Compared to the equations used to form the GFM-current (3.4) and (3.5) for the regular STATCOM which only has the q-component, the new equations for the E-STATCOM needs to be divided into the d- and q-component.
The equations for the Back-EMF is changed in the way that the Z_{virt} component is split into its R and X components resulting in the following equation for the q-component of the Back-EMF (3.8),

$$E_{EMF\_q} = (U_{ref\_prim} + I_{prim} \cdot X_T) + I_{VSC} \cdot R_{virt} + DCREG\_KP \cdot X_{virt} \quad (3.8)$$

and for the d-component only the virtual reactance and the voltage regulator contribution is added according to (3.9).

$$E_{EMF\_d} = (U_{ref\_prim} + I_{prim} \cdot X_T) - I_{VSC} \cdot X_{virt} \quad (3.9)$$

The block diagram for the calculations of the respective d- and q-components of the Back-EMF and the voltage error can be seen in Figure 3.13

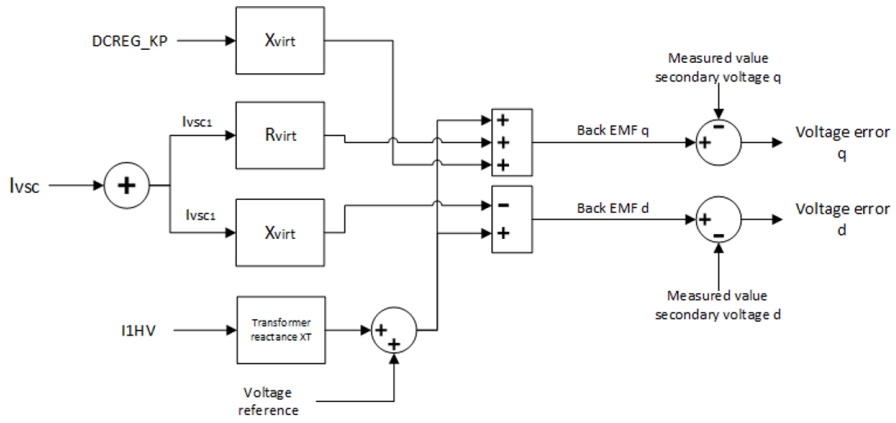

Figure 3.13: Block diagram for the d- and q-components of the Back-EMF and voltage error.

Then referring to (3.5) the GFM-current for the q-component is expressed as (3.10),

$$I_{GFM\_q} = \frac{1}{ST_{18}} \cdot \frac{U_{ERR} - I_{GFM\_d} \cdot X_{virt} - I_{GFM\_q} \cdot R_{virt}}{L_{virt}} \quad (3.10)$$

where I_{GFM_d} and I_{GFM_q} are the previous states of the d- and q-component currents that were calculated in the previous iteration of the network solution. The d-component of the current is calculated in a similar way but with a change in sign and the resistance and reactance changes place according to (3.10).

$$I_{GFM\_d} = \frac{1}{ST_{18}} \cdot \frac{U_{ERR} - I_{GFM\_d} \cdot R_{virt} + I_{GFM\_q} \cdot X_{virt}}{L_{virt}} \quad (3.11)$$

The block diagram for the calculations of the d- and q-components of the GFM-current can be seen in Figure 3.14.

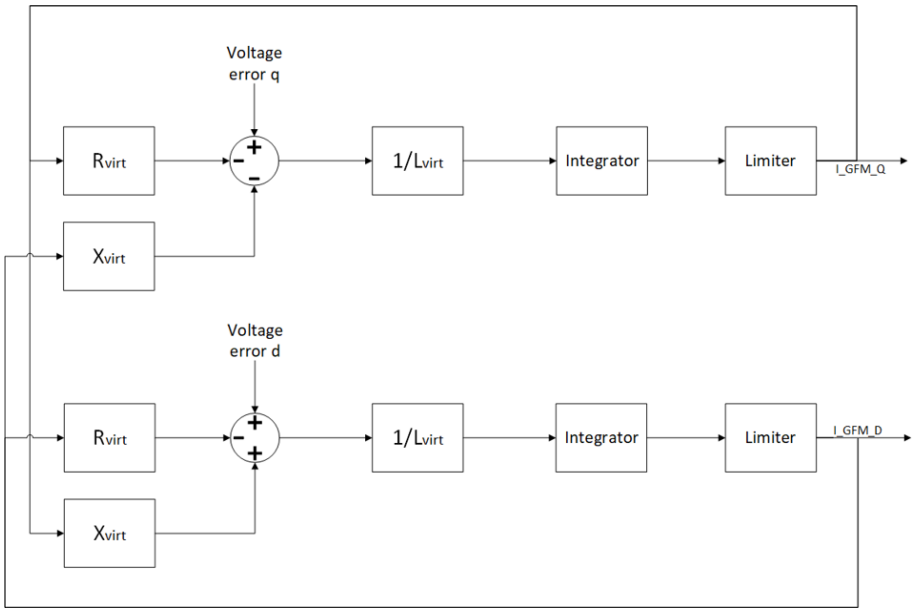

Figure 3.14: Block diagram for the d- and q-components of the GFM-current

According to Figure 3.14 the q-component, which is according to (2.36) the component that gives the reactive power in dq-coordinates, has the contribution from the DC-voltage in (3.8) and the d-component (3.9) does not. The reason for this can be seen by inserting the equations for I_{GFM_d} and I_{GFM_q} back into themselves (since they are fed back) and looking at only the contribution the d- and q-components have from the DC-voltage it is noted that the d-component has a stronger contribution from the DC-voltage compared to the q-component according to (3.12) and (3.13). Even though they both have a contribution the majority is in the d-component.

$$I_{GFM\_d} = ...\frac{X^2}{SC_{DC}L_{virt}} \cdot DCREG\_KP... \tag{3.12}$$

$$I_{GFM\_q} = ...DCREG\_KP \cdot X_{virt} - \frac{R_{virt}}{SC_{DC}L_{virt}} \cdot DCREG\_KP \cdot X_{virt}... \tag{3.13}$$

3.2.3 Synchronization to grid

However the currents described in the previous section are not the ones being injected to the network as it was for the STATCOM, they have to be modified to be able to react and respond to a change in frequency/active load in the grid. As mentioned in Section 2.7 the standard method that is used to synchronize to the grid is the PLL with addition from PSC which is the contribution from the change in active power and DC voltage. However this implementation has to be changed due to that the PLL can not be directly implemented in PSS®E and it has to be altered to work with the available measurements that can be done in PSS®E. The reason why the

PLL can not be directly implemented in PSS®E is because that it estimates the grid angle based on the three phase currents and voltages. Since PSS®E is a single phase RMS based simulation tool the angle can not be estimated according to this approach. So for this reason a simplified version of the PLL has to be constructed. Fortran which is the program used to build the model and the control system of the E-STATCOM, that is then to be used in the simulations in PSS®E, does not provide a simple way of extracting the angle at a certain bus. This means that to be able to access the voltage angle of a bus the imaginary and real part of the voltage has to be extracted and then the angle can be calculated using trigonometry. This angle is then added to the angle calculated by the PSC according to Figure 3.15.

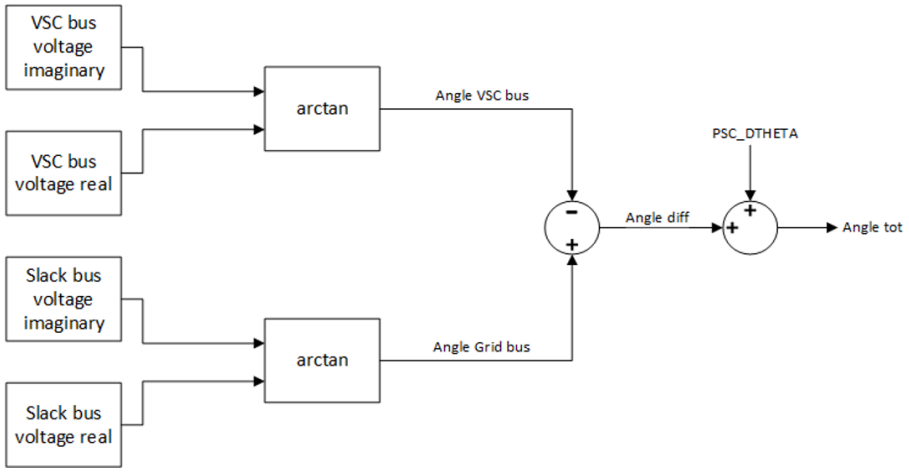

Figure 3.15: Block diagram for PLL implementation and final angle

The PSC angle is added to the PLL angle and adds the contribution from a change in active power/DC-voltage, used to synchronize the E-STATCOM to the grid and change the total angle to either allow for the E-STATCOM to inject or absorb active power from the grid, it also introduces the virtual inertia which allows for the E-STATCOM to reduce the RoCoF during disturbances in the grid. The block diagram of the calculation of this angle can be seen in Figure 3.16. The angle is calculated, by first comparing the active power from the E-STATCOM bus with the contribution from the DC-voltage DCREG_{KP} according to (3.14),

$$P_{PSC} = P_{OUT} - DCREG\_KP \tag{3.14}$$

this difference is then compared to a reference value to get the error. This is then passed through an integrator which will result in an angle that is changing depending on the active power output of the E-STATCOM according to (3.15),

$$\Delta\theta_{PSC} = \frac{1}{SGFM\_TM} \cdot P_{PSC\_ERR} \tag{3.15}$$

where the time constant GFM_TM represents the virtual inertia and is typically a very low value, allowing for the angle $\Delta\theta_{PSC}$ to respond very fast to a change in active power in the system.

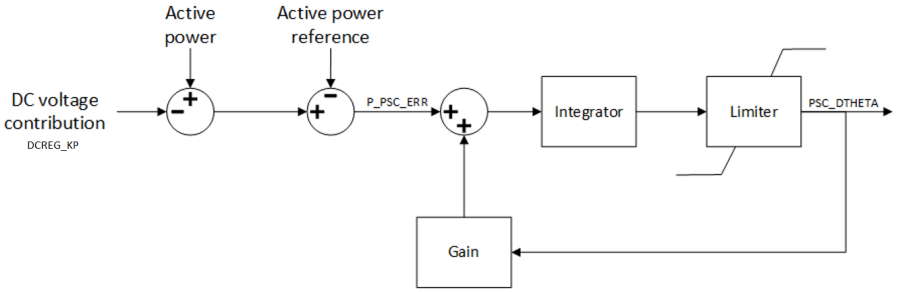

Figure 3.16: Block diagram for PSC implementation

Then the total angle is described as (3.16) and will be used together with the the d- and q-components in (3.10) and (3.11) to form the final current that will be injected to the network that will allow the E-STATCOM to provide active and reactive power support to the grid, based on the disturbances that occur. The final d- and q-components of the current are cross-coupled with the d- and q-currents in (3.11) and (3.10) according to (3.17) and (3.18) [21] .

$$\theta_{tot} = (\theta_{SLACK} - \theta_{VSC}) + \Delta\theta_{PSC} \tag{3.16}$$

$$I_{d\_final} = I_{GFM\_d} \cdot cos(\theta_{tot}) + I_{GFM\_q} \cdot sin(\theta_{tot}) \tag{3.17}$$

$$I_{q\_final} = I_{GFM\_d} \cdot sin(\theta_{tot}) + I_{GFM\_q} \cdot cos(\theta_{tot}) \tag{3.18}$$

The current from (3.17) and (3.18) will be used as variables in a function in PSS®E that calculates the complex current output array from a chosen bus used during the network solution. The function is described in (3.19)

$$I_{new} = I_{previous} - \frac{V_{bus} \cdot (I_{d\_final} + jI_{q\_final})}{|V_{bus}|} \tag{3.19}$$

where I_{new} is the output current, $I_{previous}$ is the output current from the previous iteration and V_{bus} is the voltage at the chosen bus.

3.2.3.1 Alternative approach PSC

When testing the approach described above for a change in frequency on the grid, it was found that the system does not respond to it. This is due to that the measured active power out of the E-STATCOM bus (used to calculate $\Delta\theta_{PSC}$ and DCREG_KP) only reacts to a change in active power load and not on pure frequency change. A solution to this was to instead of using the measured active power $POUT$, it was to be calculated based on a frequency depending current. This current was calculated by measuring the frequency deviation on the E-STATCOM bus and comparing that to the nominal system frequency and a frequency reference (set internally) to get the total frequency deviation according to (3.20).

$$\Delta f_{tot} = f_{ref} - (f_{nom} + \Delta f_{bus\_meas}) \tag{3.20}$$

This frequency deviation was then sent through an integrator to get the frequency depending current I_{freq_dep} and then by multiplying with the bus voltage the active power was calculated which now also has a frequency dependency (not only active power dependency). This calculated active power then replaced the measured in the calculations of $\Delta\theta_{PSC}$ and DCREG_KP. However this approach was not fully implemented and therefore not allowing for the network to converge, due to a lack of time. But the initial response when applying a frequency change with this approach will be represented in the results and discussion sections.

3.3 VMPSCAD-model

The E-STATCOM model in VMPSCAD that is to be used to compare the created E-STATCOM model in PSS®E with, has a different circuitry which will make the direct comparison between them difficult. The mayor difference that will make the direct comparison difficult is the fact that the network used to test the E-STATCOM in VMPSCAD has two E-STATCOMs in it, which also do not act identically and also have an exchange between each other. However despite these differences, comparisons regarding the general response/behavior of the various signals in the E-STATCOM can be made between PSS®E and VMPSCAD, which will indicate how the PSS®E-model is performing compared to the VMPSCAD-model.

4
Model results

The constructed model will be tested with two different disturbances/changes in the network, the first being a change in active power in increasing size (both negative and positive) and the second one being a change on the frequency on the grid. The results will include the behavior of the frequency deviation, the injected d- and q-components of the current, the bus voltage at the SVS HV bus seen in Figure A.4, the DC-voltage and active power output of the E-STATCOM during steady state and disturbance. Also some comparisons to the existing VMPSCAD-model will be made, however the circuit for the VMPSCAD-model is slightly different than that of the PSS®E-model as mentioned in Section 3.3. The system that is being used to carry out the tests on is shown in Figure A.4 located in Appendix A.2. For the first case there will be an added signal (yellow), which is to show what happens if X_{virt} and R_{virt} is not properly tuned to the system. The same behavior could be seen on the other signals as well but they were only added in the first.

4.1 Active power load change

The response of the E-STATCOM for a change in active power load, with both a positive change and negative change will be presented in this section.

4.1.1 Negative load change

The response of the E-STATCOM when a negative active power load is switched on/off to the system is presented in Figures 4.1-4.3. Where the dq-components of the final current is plotted in Figure 4.1, the DC-voltage across the energy storage and the AC-voltage on SVS HV bus seen in Figure A.4 is plotted in Figure 4.2 and the frequency deviation of the system and the active power output of the E-STATCOM is plotted in Figure 4.3. The load is switched on after one second and removed after three seconds and the response for an increase in load is compared in the plots. Where the blue signal corresponds to a load of -5 MW, the red -10 MW, the yellow -15 MW which is before the virtual impedance parameters where tuned and the purple -20 MW. In Figure 4.1 it can be seen that both i_d and i_q for all cases have an output decrease when the load is applied. However i_q's value for all cases goes towards zero over time while i_d's value for all cases turns positive and increases until a constant value of 0.05 pu is achieved for the -5 MW case, 0.1 pu for the -10 MW case, 0.15 pu for the -15 MW case and 0.2 pu for the -20 MW case. These values are relatively high compared to the initial value dip that doesn't exceed -0.04 pu for

neither of current components. When the load is removed after 3 seconds there is an increase for all cases. The increase in i_d varies for all cases where the -20 MW case has the largest increase with over 0.05 pu, the -15 MW case has an increase of approximately 0.03 pu, the -10 MW case has an increase of approximately 0.02pu and the -5 MW case has an increase of approximately 0.01 pu. After the initial increase in current the values decreases until a value of 0 pu is reached which it is for all i_d cases after 5 seconds. The yellow signal has some oscillations when the load is disconnected, both for i_d and i_q. The increase in i_q after the load is removed is similar to the decrease that appeared after the load was applied.

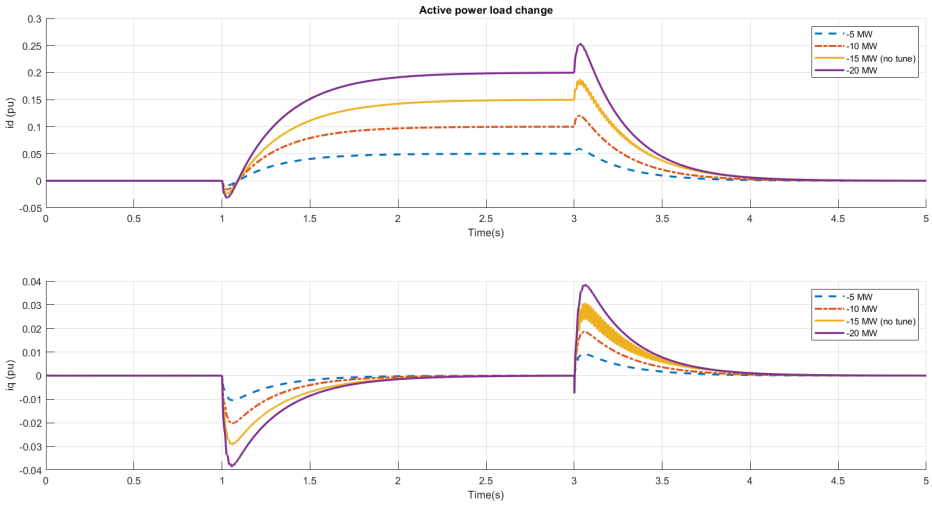

Figure 4.1: dq-components of the final current (pu) during a change in active power load (negative), the upper plot is the d- and the lower is the q-component. Blue (-5 MW), red (-10 MW), yellow (-15 MW) and purple (-20 MW)

The behavior of the DC-voltage during a negative load can be seen in Figure 4.2. After the load is applied there is a voltage increase for all cases but they stabilize at different values. For the -5 MW case the voltage stabilizes at 1.2 pu, for the -10 MW case the voltage stabilizes at 1.35 pu and for the -20 MW case the voltage stabilizes at 1.53 pu. After the load is removed the voltage decreases and goes towards its initial value at 1.17 pu for all cases. A value which they reach at the same time.

The AC-voltage can be seen in Figure 4.2. After the load is connected there is a jump in voltage up to around 1.00035 pu for the -20 MW case, but for the other cases it starts decreasing immediately. Then the -20 MW case quickly decreases down to 0.9993 pu and from that point it increases until it reaches 1 pu at around 2 s, which all cases reach at the same time. Then when the load is disconnected there is a drop in the -20 MW case down to 0.9993 pu and then it jumps up to 1.00045 pu, whereas for the other cases it has a direct increase in voltage and then all cases move towards 1 pu again and reaches it after around 4 s.

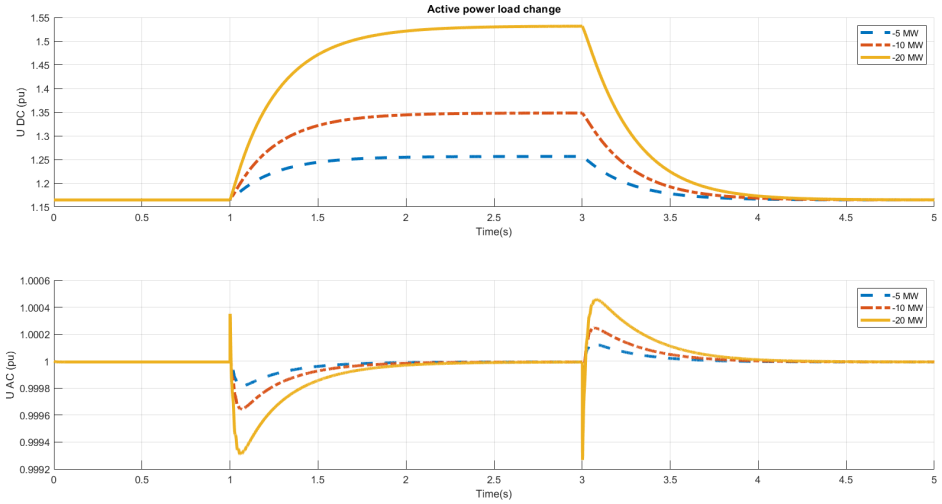

Figure 4.2: DC-voltage (pu) across the energy storage and AC-voltage at bus SVS HV during a change in active power load (negative). Blue (-5 MW), red (-10 MW) and yellow (-20 MW)

The frequency deviation at the E-STATCOM bus is shown in the upper graph of Figure 4.3. The frequency deviation increases for all cases when the load is applied. For the case with a -5 MW load the frequency increases and stabilizes at 0.0006 pu, with a -10 MW load the frequency increases and stabilizes at 0.0015 pu an with a -20 MW load the frequency increases and stabilizes at 0.0036 pu. The lower half of Figure 4.3 shows the active power output from the E-STATCOM. From the plot it can be seen that when the load is applied the E-STATCOM immediately increases its active power output for all cases. When a -5 MW load is applied the output increases to 0.05 pu, with a -10 MW load the output increases to 0.1 pu and with a -20 MW load the output increases to 0.2 pu. The output begins to decrease a short period after the load is applied which and the output goes towards the initial value of 0 pu, this happens for all the cases. When the load is removed the same behavior occurs for all cases but instead for a increase in active power output the output decreases. With a -5 MW load the output decreases to -0.05 pu, with a -10 MW load the output decreases to -0.1 pu and with a -20 MW load the output decreases to -0.2 pu. After immediate decrease the output begins to go towards the initial value for all cases.

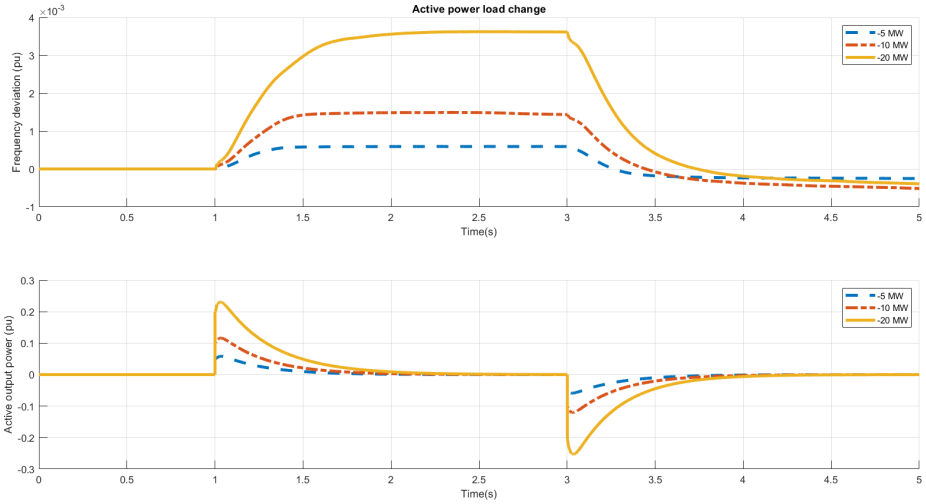

Figure 4.3: Frequency deviation (pu) and active power output (pu) from E-STATCOM during a change in active power load (negative), the upper plot is the frequency deviation and the lower is the active power output. Blue (-5 MW), red (-10 MW) and yellow (-20 MW)

In order to discuss some of the behaviors of the E-STATCOM's signals the total angle θ_{tot} and parameters I_{GFMd} and I_{GFMd} needs to be plotted as well and can be seen in Figure 4.4.

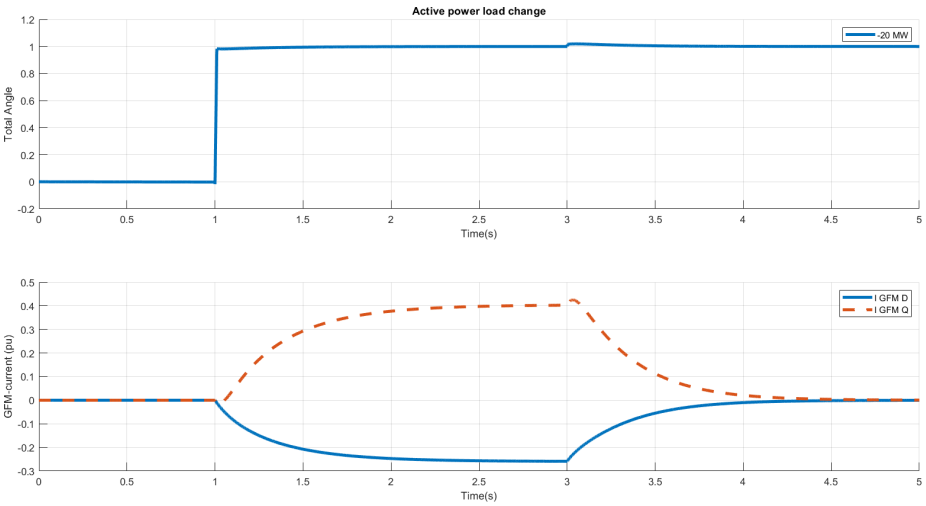

Figure 4.4: The total angle θ_{tot} and I_{GFMd} (blue) and I_{GFMq} (red) during a negative load change

4.1.2 Positive load change

The response of the E-STATCOM when a positive active power load is switched on/off to the system is presented in Figures 4.5-4.7. Where the dq-components of

the final current is plotted in Figure 4.5, the DC-voltage across the energy storage is plotted in Figure 4.6 and the frequency deviation of the system and the active power output of the E-STATCOM is plotted in Figure 4.7. The load is switched on after one second and removed after three seconds and the response for an increase in load is compared in the plots. Where the blue signal corresponds to a load of 5 MW, the red 10 MW and the yellow 20 MW.

The current components i_d and i_q are plotted in Figure 4.5 where i_d is shown in the upper half and i_q in the lower half. It is shown in the plot that i_d decreases in every load case but the slope of the curve and the maximum deviation varies. For the case with a 5 MW load i_d decreases for approximately 0.6 seconds until the current reaches -0.05 pu. For the cases with a 10 MW and 20 MW load i_d has a similar behavior but the current stabilizes at -0.1 pu respectively -0.2 pu. When the load is removed i_d increases until it reaches the initial value of 0 pu for all cases. i_q on the other hand barely has a response from any of the loads. The current decreases to -0.01 pu for the most extreme case of 20 MW. When the load is removed a spike reaches 0.033 pu for the most extreme case.

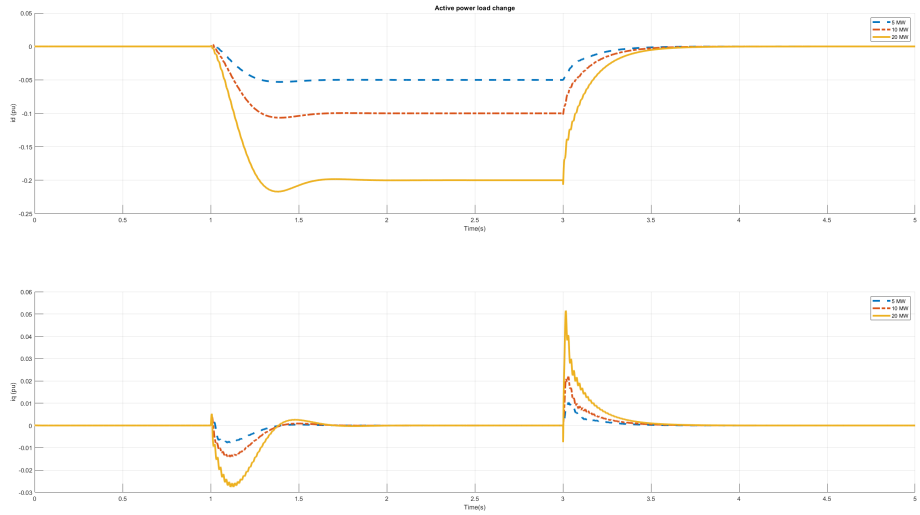

Figure 4.5: dq-components of the final current (pu) during a change in active power load (positive), the upper plot is the d- and the lower is the q-component. Blue (5 MW), red (10 MW) and yellow (20 MW)

Figure 4.6 shows the DC-voltage at the energy storage UAC and AC-voltage at HV-side of the transformer UAC when a active power load is applied. The DC-voltage UDC, upper half of the Figure, has a initial value of 1.165 pu before the load is applied. When the load is applied UDC decreases in every case but the slope of the curve and maximum deviation varies. For the case with a 5 MW load UDC decreases until it reaches 1.125 pu after 0.6 seconds, with a 10 MW load UDC decreases until it reaches 1.09 pu after 0.6 seconds and with a 20 MW load UDC decreases until it reaches 1.01 pu after 0.6 seconds. When the load is removed UDC increases for every case until it reaches the initial value of 1.165 pu after 1 second.

The lower half of Figure 4.6 shows the behavior of UAC. The initial value is 1 pu and after the load is applied there are small deviations of 0.0007 pu for a short period of time. Then UAC goes to 1 pu and holds that value until the load is removed at 3 seconds. A spike occurs that reaches 1.0012 pu for the worst case and after the spike UAC decreases towards 1 pu.

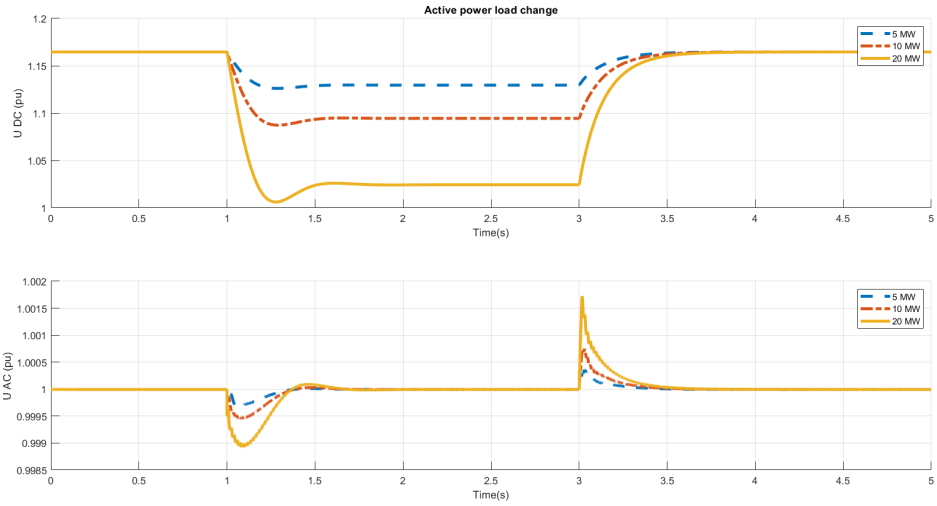

Figure 4.6: DC-voltage (pu) at the energy storage during a change in active power load (positive). Blue (5 MW), red (10 MW) and yellow (20 MW)

The frequency deviation is shown in the upper half of Figure 4.7 for three different cases. After the load is applied at 1 second the frequency deviation decreases for every case but the slope of the curve and maximum deviation varies. For a load with 5 MW the frequency deviation decreases for the whole period the load is applied and reaches a maximum deviation of -0.0005 pu right before the load is removed at 3 seconds. When the 10 MW load is applied the frequency deviation decreases for the whole period the load is applied and reaches a maximum deviation of -0.001 pu right before the load is removed at 3 seconds. For the 20 MW load the frequency deviation decreases for the whole period the load is applied and reaches a maximum deviation of -0.0015 pu right before the load is removed at 3 seconds.The signals does not reach their initial value of 0 pu for any case, instead the deviation start to decrease. The active power output $POUT$ is shown in the lower half of Figure 4.7 for three different cases. When the load is applied an instant decrease in active power occurs for all cases. For the case with a 5 MW load $POUT$ decreases to -0.05 pu, with a 10 MW load $POUT$ decreases to -0.1 pu and with a 20 MW load $POUT$ decreases to -0.2 pu. After the instant decrease $POUT$ begins to increase towards its initial value of 0 pu for all cases. When 0 pu is reached the value is constant until the load is removed which results in a instant increase in active power at 3 seconds. For the case with a 5 MW load $POUT$ decreases to 0.05 pu, with a 10 MW load $POUT$ decreases to 0.1 pu and with a 20 MW load $POUT$ decreases to 0.2 pu. After that $POUT$ begins to decrease for all cases until 0 pu is reached.

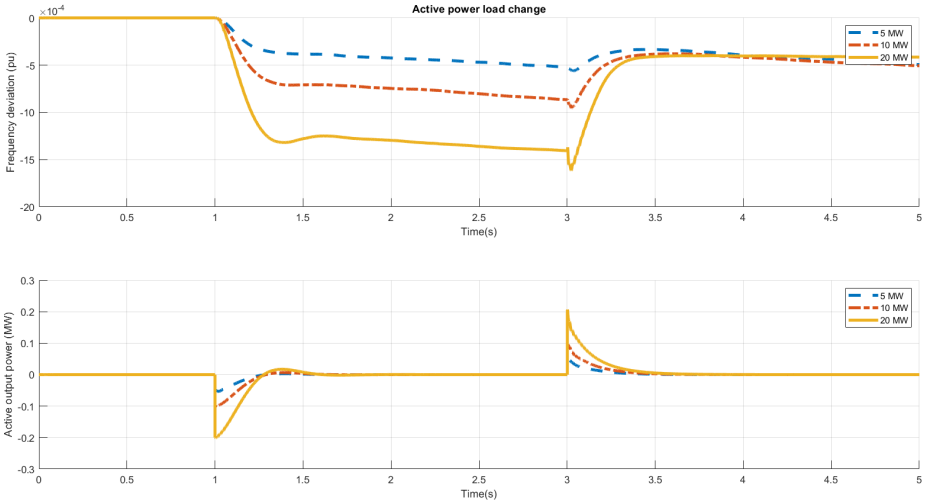

Figure 4.7: Frequency deviation (pu) and active power output (pu) from E-STATCOM during a change in active power load (positive), the upper plot is the frequency deviation and the lower is the active power output. Blue (5 MW), red (10 MW) and yellow (20 MW)

4.2 Frequency change on the grid side

The E-STATCOM's response to a change in frequency on the grid side is presented. Both with the approach described in Section 3.2.3 which is the approach used for the active power change as well and also the approach described in Section 3.2.3.1. Where the first approach uses the measured active output power of the E-STATCOM bus in its calculations and the other approach is based on a calculated active output power as described in Section 3.2.3.1.

4.2.1 Measured active output power

The response of the E-STATCOM to a ramping frequency change on the grid from 1 to 0.99 in pu which represents a change from 50 to 49.5 in Hz, when using the approach that measures the output power on the E-STATCOM bus is presented. The frequency change is applied after one second and reaches its final value after 1.5 seconds. Here the dq-components of the final current can be seen in Figure 4.9, the DC- and AC-voltage in Figure 4.10 and the frequency deviation and active power output in Figure 4.8.

The upper half of Figure 4.8 shows how the frequency deviation drops from 0 pu to -0.1 pu during the period from 1 second to 1.6 seconds. The frequency drop was created in order to see how other parameters responded to it. The lower half of Figure 4.8 shows the active power output *POUT*. The signal is close to 0 pu both before and after the frequency change apart from some noise that appear at 1 second.

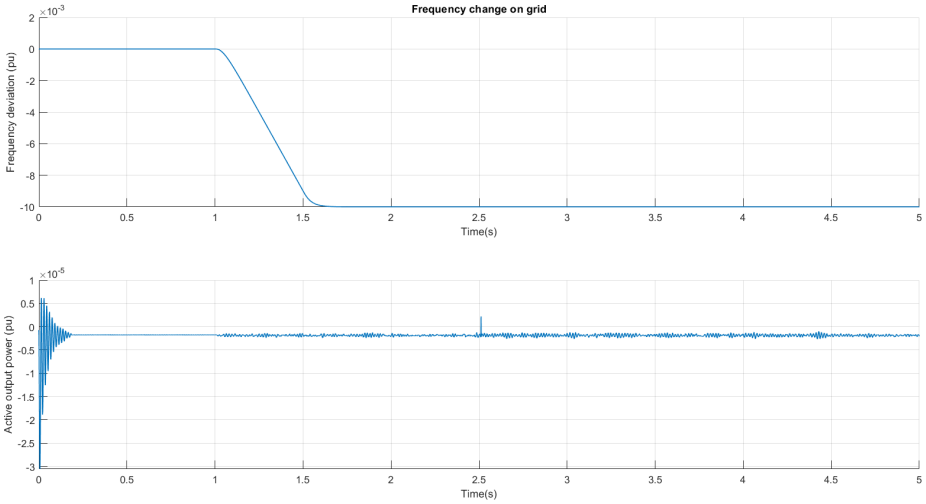

Figure 4.8: Frequency deviation (pu) and active power output (pu) from E-STATCOM during a frequency change (50 to 49.5 Hz) on the grid side, the upper plot is the frequency deviation and the lower is the active power output.

Figure 4.9 shows the behavior of the current components i_d and i_q. According to the plot neither i_d or i_q appear to respond to the frequency change. Both of the current components has a constant value apart from some noise that appear at 1 second.

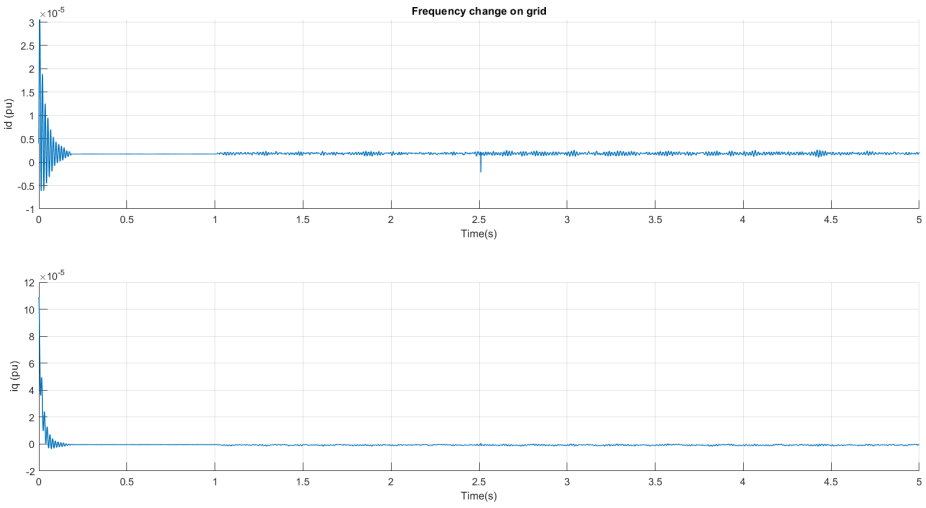

Figure 4.9: dq-components of the final current (pu) during a frequency change (50 to 49.5 Hz) on the grid side, the upper plot is the d- and the lower is the q-component.

The DC-voltage UDC and AC-voltage UAC are shown in Figure 4.10. Neither of the signals appear to respond to the frequency change. Their values are constant during the whole period but some noise appear in UAC after 1 second.

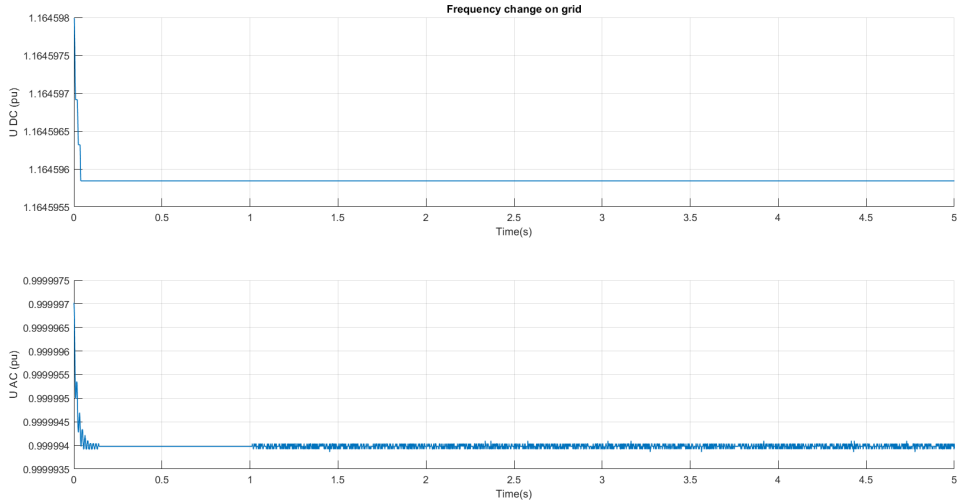

Figure 4.10: DC-voltage (pu) at the energy storage and AC-voltage (pu) at SVS HV bus during a frequency change (50 to 49.5 Hz) on the grid side, the upper plot is the DC and the lower is the AC.

4.2.2 Calculated active output power

The response of the E-STATCOM to a ramping frequency change on the grid from 1 to 0.99 in pu which represents a frequency change from 50 Hz to 49.5 Hz, when using the approach that calculates the output power on the E-STATCOM bus instead of measuring it. The frequency change is applied after one second and reaches its final value after 1.5 seconds. Here the dq-components of the final current can be seen in Figure 4.12, the DC- and AC-voltage in Figure 4.13 and the frequency deviation and active power output in Figure 4.11.

The frequency deviation shown in the upper half of Figure 4.11 begins to decrease after 1 second. The frequency drop was created in order to see how other parameters responded to it. The active power output *POUT* shown in the lower half of Figure 4.11 begins to increase 0.1 seconds after the frequency ramp began. *POUT* continues to increase while the frequency deviation decreases and reaches at least a value of 0.73 pu.

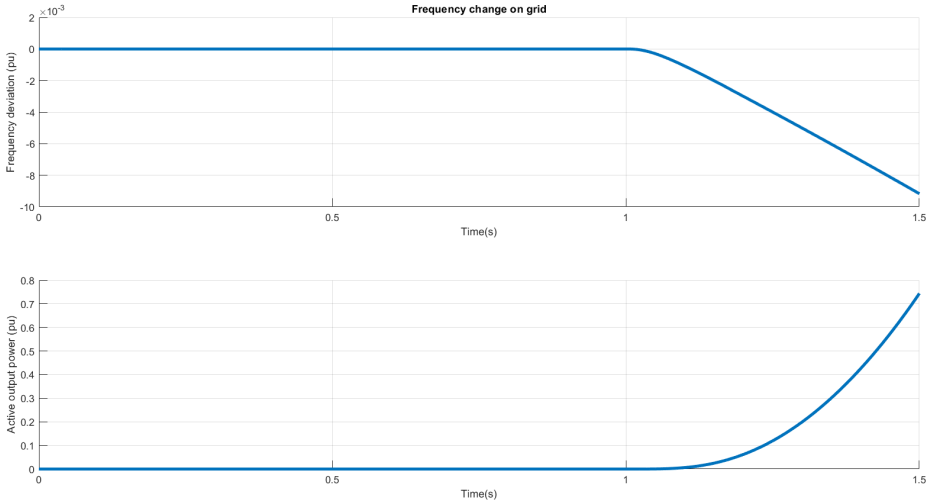

Figure 4.11: Frequency deviation (pu) and active power output (pu) from E-STATCOM during a frequency change (50 to 49.5 Hz) on the grid side, the upper plot is the frequency deviation and the lower is the active power output.

The current component i_d shown in the upper half Figure 4.12 begins to respond to the frequency ramp 0.1 seconds after the frequency ramp began and i_d increases from its initial value of 0 pu to 0.11 pu. The other current component i_q shown in the lower half begins to decrease 0.1 seconds after the frequency ramp began. i_q decreases until it reaches a value of -0.078 pu.

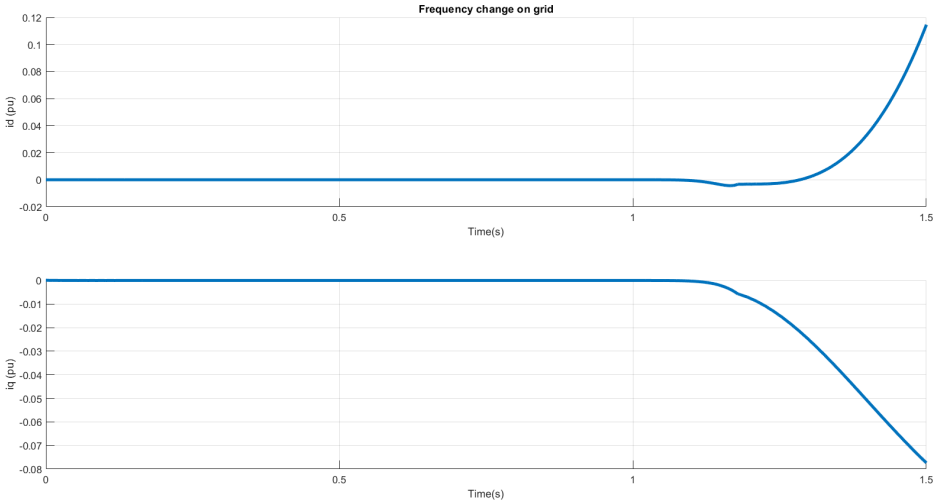

Figure 4.12: dq-components of the final current (pu) during a frequency change (50 to 49.5 Hz) on the grid side, the upper plot is the d- and the lower is the q-component.

The DC-voltage UDC which has an initial voltage of 1.175 pu begins to increase after the frequency ramp began and reaches a value of at least 1.62 pu. This is

shown in the upper half of Figure 4.13. The AC-voltage UAC begins to decrease and the deviation from the initial value of 1 pu is relatively small.

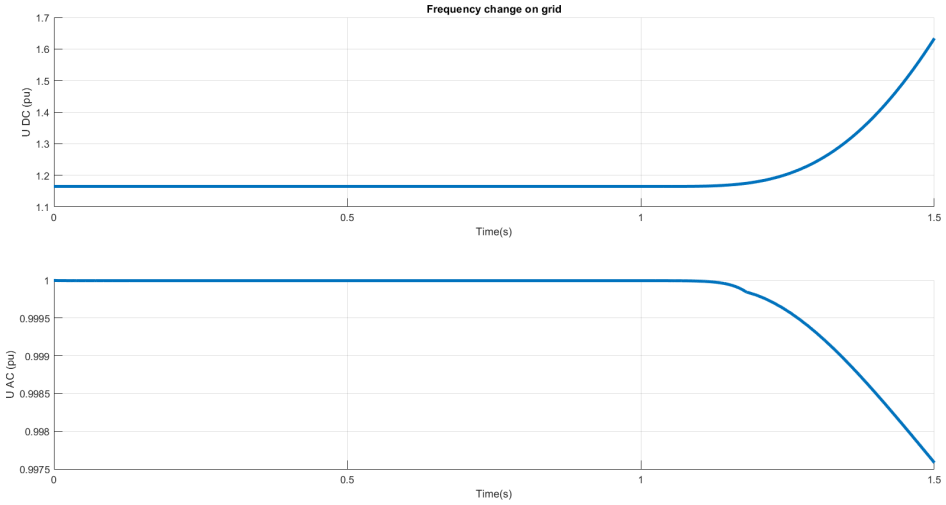

Figure 4.13: DC-voltage (pu) at the energy storage and AC-voltage (pu) at SVS HV bus during a frequency change (50 to 49.5 Hz) on the grid side, the upper plot is the DC and the lower is the AC.

4.3 Comparison to VMPSCAD

The comparison between the E-STATCOM model in PSS®E and the E-STATCOM model in VMPSCAD is represented in Figures 4.14 and 4.15. This comparison is made during an active power load of 20 MW, where it is switched on at one second and switched off after two seconds. The PSS®E-model is the blue signal and the VMPSCAD-model is the red signal, the d-component is plotted in the upper graph and q-component in the lower in Figure 4.14 and the active power is plotted in the lower graph and the frequency is plotted in the upper graph in Figure 4.15.

The upper graph in Figure 4.14 shows that when the load is applied at 1 second the PSS®E-model decreases for 0.5 seconds until the current reaches a value of -0.2 pu. The VMPSCAD-model has an instant decrease to -0.05 pu when the load is applied and then begins to increase towards its initial value of 0 pu. When the load is switched off at 2 seconds the PSS®E-model begins to increase towards its initial value of 0 pu while the VMPSCAD-model has an instant increase to 0.05 pu. After the instant increase the current decrease until it has reached 0 pu.

In the lower graph in Figure 4.14 the PSS®E-model has a relatively small initial increase and begins to oscillate after the load is applied. The current decreases towards its initial value of 0 pu after the initial increase and reaches 0 pu after 0.5 seconds. The VMPSCAD-model decreases to -0.04 pu and then increases to 0 pu before the load is applied. After the load is applied the VMPSCAD-model has a drop down to -0.018 pu and then increases until it reaches a maximum value of 0.02

pu before it stabilizes at 0.018. When the load is removed the PSS®E-model drops down to -0.012 pu and then begins to oscillate with a decreasing amplitude. The VMPSCAD-model has a spike that reaches 0.04 pu and then decreases to 0 pu.

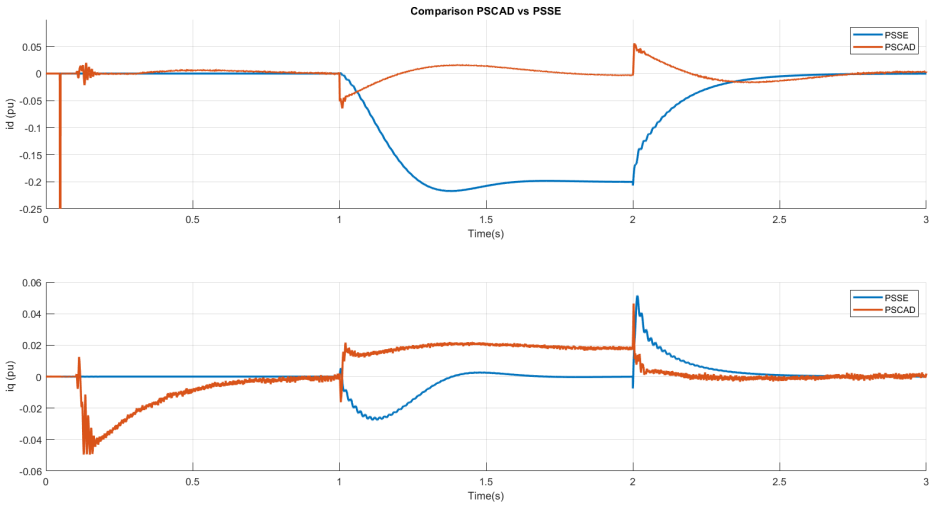

Figure 4.14: dq-components of the final current in the PSS®E-model (blue) compared with the VMPSCAD-model(red), during a change in active power load of 20 MW. Where the upper graph is the d-component and the lower is the q-component.

In the upper graph in Figure 4.15 the frequency in PSS®E (blue) starts to slowly decrease at 1 second when the load is applied and then starts to stabilize at around 49.92 Hz. The VMPSCAD-model (red) has a faster drop on the frequency to around 49.95 before it quickly goes back to oscillating around 50 Hz. When the load is disconnected at 2 seconds the frequency in PSS®E starts to increase until it stabilizes around 49.98 Hz, the VMPSCAD-model has a quick increase to around 50.05 Hz before it goes back to oscillating around 50 Hz again.

The lower graph in Figure 4.15 shows that when the load is applied at 1 second the active power output of the E-STATCOM in PSS®E (blue) drops to -20 MW and after that increases to reach its starting value of 0 MW. when the load is disconnected at 2 seconds the output jumps up to 20 MW and then starts decreasing until it reaches its starting value again of 0 MW. The output power of the E-STATCOM in VMPSCAD (red) has a similar behavior regarding the drop at 1 second and the jump at 2 seconds, however there are some oscillations. It goes up to 6 MW after dropping to -20 MW and then moving back to small oscillations around 0 MW, then it goes down to -6 MW after jumping up to 20 MW and then moving back to oscillating around 0 MW. The active output power plotted for the VMPSCAD-model is the contribution from both of the E-STATCOMs mentioned in Section 3.3.

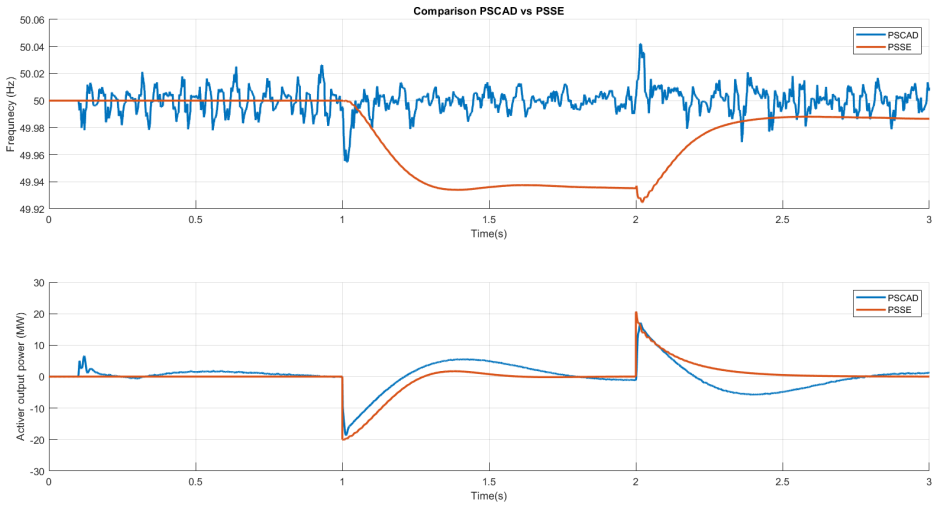

Figure 4.15: Active power from the E-STATCOM in the PSS®E-model (blue) compared with the VMPSCAD-model(red) and frequency in the PSS®E-model (red) compared with the VMSPCAD-model (blue), during a change in active power load of 20 MW. Where the upper graph is the frequency and the lower is the active power output.

4.4 Under voltage

The reactive power support from the E-STATCOM is tested by applying a fault on the system. The fault is an inductive fault with the size of 0.064 H, therefore causing a drop in the system voltage. The response of the E-STATCOM can be seen in Figure 4.16 where the d- and q-component of the current can be seen and in Figure 4.17 the reactive power output from the E-STATCOM as well as the voltage on the SVS HV bus in Figure A.4 in Section A.2.

4.4.1 Current components

The current component i_d shown in the upper graph of Figure 4.16 has a spike when the fault is applied at 0.5 seconds that reaches a value greater than 1 pu and then begins to oscillate with a decreasing amplitude until it reaches its initial value of 0 pu after 0.55 seconds. The other current component i_q shown in the lower graph has a instant increase that reaches 2 pu and then begins to oscillate. i_q stabilizes after 0.54 seconds at a value 1.3 pu. When the fault is cleared after 0.6 seconds i_d begins to oscillate and reaches a peak value of 1.1 pu. i_d stabilizes at 0 pu 0.1 seconds after the fault is cleared. i_q on the other hand drops down to 0 pu and then begins to oscillate with a peak amplitude of 2 pu. The current then decreases and stabilizes at its initial value of 0 pu after 0.72 seconds.

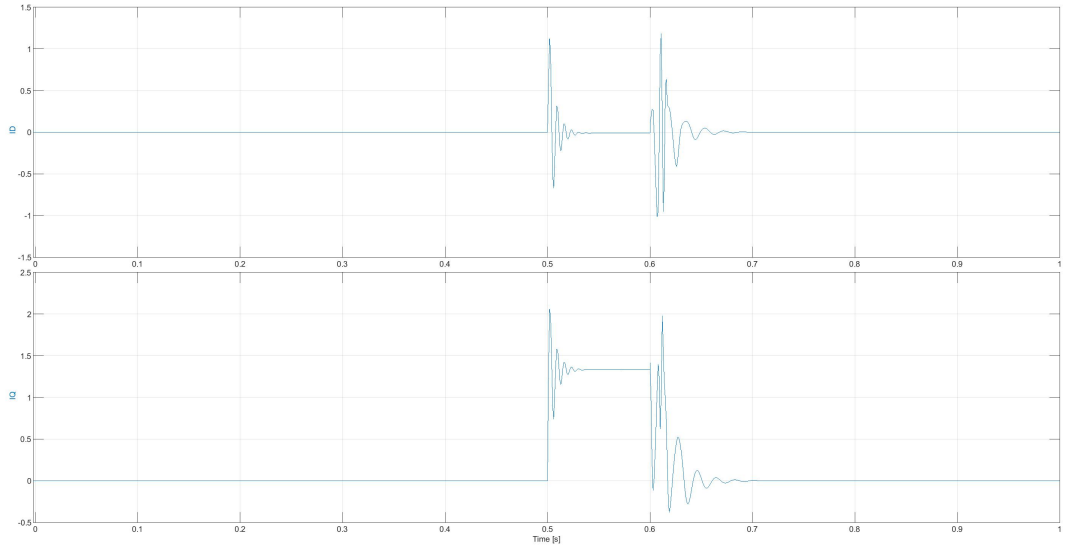

Figure 4.16: dq-components of the final current (pu) during an inductive fault in the system, the upper plot is the d-component and the lower is the q-component.

4.4.2 Voltage and reactive power

The upper graph of Figure 4.17 shows the AC-voltage on the SVS HV bus UAC. When the fault is applied at 0.5 seconds UAC drops to 0.4 pu and holds that value for the entire period of the fault. The lower graph shows the reactive power output $QOUT$ which has a instant increase to 0.4 pu when the fault is applied and then holds that value for the entire period of the fault. When the fault is cleared at 0.6 seconds UAC has an instant increase to 1.02 pu and then has a value variation until it stabilizes at its initial value of 1 pu. $QOUT$ begins to oscillate when the fault is cleared with a peak amplitude of 1.1 pu. Then the amplitude decreases over time until the reactive power output goes back 0 pu after 0.72 seconds.

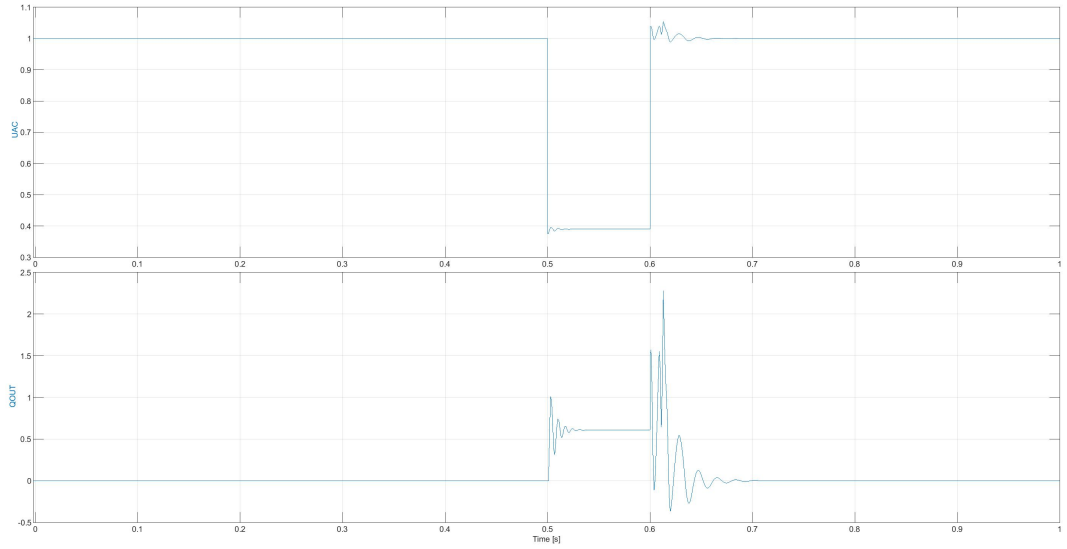

Figure 4.17: AC-voltage on the SVS HV bus and the reactive power output of the E-STATCOM during an inductive fault in the system, the upper plot is the AC-voltage and the lower is the reactive power output.

5
Discussion

The behavior of the different signals in the E-STATCOM during the active power load change, the frequency change on the grid side and the fault will be discussed based on what could be expected and how well the E-STATCOM handles the various disturbances and changes in the network. Discussions on how the choices made when constructing the E-STATCOM effects the results and the behavior of the E-STATCOM during the various events will also be made in this Chapter. Also discussions will be made based on how PSS®E is constructed and how that affected our results.

5.1 Negative load change

When the negative active power load is applied to the system after 1 second there is a decrease at first in both i_d and i_q shown in Figure 4.1. This happens because at the moment the load is applied the variable I_{GFMd} (3.11) and I_{GFMq} (3.10) has a value close to 0 pu before the load is applied and U_{ERR} (3.3) has a negative value. So when PSS®E does its first iteration to calculate (3.10) and (3.11) the output will have a negative value until I_{GFMd} and I_{GFMq} begins to increase. When they have done so i_d and i_q converges to a final value that however is not expected for all cases. When a negative active power load is applied the E-STATCOM is expected to absorb active power due to that the total generation of active power is now bigger than the consumption. Therefore i_d should be expected to be negative during the time the load is applied, according to (2.35). The reason why i_d becomes positive instead is caused by the angle $\Delta\theta_{PSC}$. Which when calculated by the integrator as in Figure 3.12 jumps to its limit of one directly when the load is applied and stays there. This will then cause the total angle that is calculated according to (3.16) which is used in (3.17) to stay constant at 1, which in turn will make i_d positive instead of negative. Due to that cos(1) has a smaller positive value than sin(1) has a negative value and the variables I_{GFMd} and I_{GFMq} being close to equal during that time period will lead to i_d being positive instead of the expected negative. The total angle and I_{GFMd} and I_{GFMq} can be seen in Figure 4.4. This is something that has to be looked into for future work. The reason why the angle does this is also due to the fact that the active power jumps up when the load is connected and then decreases instead of decreasing from the beginning to recover the frequency. Which will cause the angle $\Delta\theta_{PSC}$ to move in the opposite direction compared to what is expected, due to the behavior of the integrator. A possible solution to this was introduced in Section 3.2.3.1 and simulations from this solution will be shown later. However this

behavior still manages to slow down the frequency change during disturbance which is discussed later.

When the load is removed at 3 seconds i_d and i_q increases at first. This is because of the same reason that the value decreases when the load is applied. U_{ERR} increases when the load is removed which means that I_{GFMd} and I_{GFMq} will increase in the next iteration. After that i_d and i_q converges to 0 pu which is expected since that now that the load is removed there should not be a need to inject active or reactive current. The reason why i_q (referred to as reactive current) has a response at all to an active power load change is due to the reason that the d- and q-components of the current are cross-coupled as was described when constructing them earlier and can be seen in (3.17) and (3.18). But in the end the q-component has a very small contribution from the DC-side and also therefore has less of a reaction to an active power load change, it only responds to the initial change that occurs when the load is connected/disconnected, and then when stabilized the components in (3.18) cancel out each other.

The purple signals in Figure 4.1, is an example of what happened before the parameters X_{virt} and R_{virt} in (3.11) and (3.10) where properly tuned to fit the connected the system. There were oscillations occurring directly when a load was connected or disconnected, showing the importance of these parameters in order to also have a stable grid during disturbances or changes. The tuning of the parameters where done by trial and error, in order to get the best overall fit for all cases.

The DC-voltage UDC in Figure 4.2 shows that the voltage is constant until the load is applied which is how it should work according to the block diagram in Figure 3.12. After the load is applied the equation for UDC changes so that it now is a function of the active power. So if the active power output $POUT$ shown in Figure 4.3 changes then UDC should change as well which is what happens for all cases. Since the load that is applied is negative the super-capacitance has to absorb (charge) active power to balance the network and to absorb active power the voltage across the energy storage will increase, which is what happens for all the cases. The AC-voltage UAC has a maximum deviation of 0.0007 pu and the behavior of the AC-voltage correlates to the behavior of i_q during load change, this is expected since i_q is the current that controls the reactive power and therefore also the voltage in the system. The exception is for the -20 MW case where there is a jump when the load is connected and a drop when the load is disconnected. The reason behind this is the drop that occurs in i_d directly when the load is connected and the jump when the load is disconnected. Since the d- and q- components are cross-coupled they will have some influence on each other, and since the the magnitude of these changes in i_d are of the same or not even larger than for i_q for a short duration, the initial behavior of the voltage will depend on i_d but then i_q takes over and will contribute as expected. The AC-voltage is fully recovered from its small deviations that occur during load change.

The frequency deviation increases when the negative active power is applied. Because the negative load results in less load in the grid, while the power in to the system is the same and therefore the frequency increases as it does in Figure 4.3 for all cases. The deviation increases until it converges at a positive value in all cases. That means that the frequency does not come back to its initial value of 50

Hz during the disturbance. So the E-STATCOM's output $POUT$ is only supplying enough active power to reduce the frequency change and then keep it at a constant level over the period the load is applied. Instead when the load is removed $POUT$ instantly decreases as a result and then increases towards 0 pu. Because $POUT$ is active again the frequency deviation decreases but it does not converge at 0 pu as it should. However the deviation from 0 is relatively small. The reason why the frequency deviation keeps decreasing past 0 pu, is due to that the E-STATCOM responds to active power change. Therefore when the load is disconnected the E-STATCOM stops contributing with active power, even though the frequency has not fully stabilized at its nominal value. So even if the total angle used in (3.17) and (3.18) is not zero I_{GFMd} and I_{GFMq} however is, which will lead to no more power injection to the system.

5.2 Positive load change

When the positive active power load is applied to the system after one second, i_d decreases until it reaches a steady state value which is depending on the size of the load and increases back to zero when the load is disconnected and can be seen in Figure 4.5. Here i_q has some oscillations during the transitions when the load is connected and disconnected but during the time it is connected it is zero which is expected since no reactive power support is needed. The reason why there are oscillations for i_q during the positive load change and not the negative load change, is linked to the tuning of the virtual impedance parameters. Since they where tuned using trial and error some sacrifices had to be made and it ended up being these oscillations since they occur for such a short moment. As was discussed for i_d in the negative load case, the same principle is also true for the positive load case. However it is expected that i_d should be positive since the E-STATCOM should inject active power to the grid since there is an increase of load in the system. The same reason as discussed for the negative load case is true for the positive, except that the angle $\Delta\theta_{PSC}$ now goes down to a value of -1 and this will cause i_d to become negative instead of the expected positive, using the same argument and equations as before.

The DC-voltage UDC in Figure 4.6 shows that the voltage is constant when no load is connected which is to be expected since no active power is needed. When the load is connected after one second the voltage across the energy storage drops (the super-capacitance is discharged) in order to be able to supply active power to the network and then it stays at a constant value depending on the size of the load (higher load, higher voltage drop), then when the load is disconnected the DC-voltage goes back (charges) to its nominal value. Which is expected since no active power needs to be generated. The AC-voltage has a maximum deviation of 0.0005 pu which occurs during the disconnection of the load, so there is some influence on the voltage, however this is due to the oscillations that occur in i_q when the load is connected and disconnected.

The frequency deviation in Figure 4.7 decreases for all cases when a positive active power load is connected to the system, this is expected since the system now has more consumption than generation of active power. The frequency deviation decreases

until it converges at a negative value in all cases, meaning that it does not come back to its initial value of 50 Hz during the time the load is connected. Which means that the E-STATCOM is only able to output enough active power to slow down the frequency change and minimize the deviation, but not move it back to its nominal value during the time the load is connected. When the load is disconnected after three seconds the frequency starts increasing towards its nominal value, however it does not completely reach it, though the deviation from nominal is small. The reason why the frequency does not move back exactly to its nominal value, is connected to that the system responds on the active power output of the E-STATCOM bus and when the load is disconnected and the output has reached zero the system stops producing active power, even though at this time the frequency has not fully recovered to its nominal value. How to possibly solve this issue is mentioned in Section 3.2.3.1 and is something that has to be developed and tested further in future work.

5.3 Discussion on Frequency change on the grid side

Discussion on how the E-STATCOM responds to a frequency change on the grid will be based on the signals presented in Section 4.2.2 and will contain the solution used in previous discussions where the system responds on the measured active power output on the E-STATCOM bus, but also an alternative solution where the active power is calculated according to Section 3.2.3.1. Although this solution was not fully developed the initial response of it will be discussed to indicate how it is responding and what to be done for future work.

When using the measured *POUT* and applying a frequency drop from 1 to 0.99 pu over 0.6 seconds on the grid as seen in Figure 4.8, the system does not respond at all besides some small noises which can be neglected as can be seen in Figures 4.8 - 4.10. Why the system does not respond has been discussed for the frequency deviation during load changes. It is because when only a frequency change is applied there is no direct change in active power and therefore the system will not start injecting or absorbing active power to the system in order to respond to the frequency change. Discussions on how PSSE is constructed and how that affects the system during a frequency change will be discussed in Section 5.3.1.

However an alternative to the measured active power was introduced in Section 3.2.3.1, where instead of reacting to a change in active power it reacts to a change in frequency. This method was not fully developed but the initial response of it will be shown, in order to show that the idea behind it is the correct way to move forward when in the future working on a finalized product. For this method the frequency is decreased from 1 to 0.99 pu during 0.5 seconds as can be seen in Figure 4.11, where in the same Figure the active output power can be seen increasing after approximately 0.1 seconds. The response time of the output power can be changed by changing the time constant of the integrator used to calculate the frequency reference current. The initial response of the output power is to increase, which is desired for the E-STATCOM to be able to restore the frequency and also decrease

the RoCoF. This is however the opposite initial response compared to the positive load case discussed before, where the output power quickly drops when the load is connected and then starts increasing. The reason for this is that when there is only a frequency change the system does not see any drop in active power initially and can therefore start generating active power immediately. Also as mentioned they respond on different inputs which will result in different actions taken. In Figure 4.12 the d- and q-components of the current can be seen, where it is noted that i_d starts increasing which is desired in order for the E-STATCOM to inject active current and also therefore active power, it also follows the behavior of the active power output which is expected since i_d is the active current which controls the output power. i_q is decreasing and if compared to the positive load case where the frequency also drops, it can be noted in Figure 4.5 that i_q initially increases in that case.

However the positive load case can not be directly compared, even though the frequency drops, the active power does not drop in the frequency case. Also in the positive load case the measured active power output is used, and therefore responds with an immediate drop when the load is connected, but for this method the output power responds directly to a frequency change which will allow for a direct response and increase in active power when the frequency is decreasing in the system. Therefore it indicates that this method will be better fitted to move back the frequency to its initial value when there is disturbance on the grid, not just only slow down the RoCoF and stabilize the frequency which the measured active power method does.

The DC-voltage seen in Figure 4.13 is increasing as its initial response, which is not desired but expected since the calculation of the DC-voltage seen in Figure 3.12, takes the output power as input which will lead to an increase in DC-voltage when the output power is always positive. Therefore if going forward with the development of this method the equations for the DC-voltage will have to be altered to respond in the opposite direction of the active power output. The AC-voltage can be seen dropping which follows the behavior of i_q which is expected since i_q is the current that controls the reactive power in the system and therefore also the voltage.

5.3.1 PSS®E related issues regarding frequency change

In a simulation tool such as PSS®E, any model that is defined by the user is interfaced with the software just by a positive sequence current source with real and imaginary parts. PSS®E does not provide the user with anything else than a positive sequence current phasor to interface with the main solution engine of the software.

In a real system when the grid frequency changes the PLL will calculate a phase angle correction which will than impact the measured frequency and that will in turn change the measurements of the primary and secondary side voltages during a frequency change. These changes in the measured voltages based on the grid frequency will impact both the active and reactive power ((3.17) and (3.18) in terms of current references). Moreover, the PSC which adds the contribution from changes on the DC side or in active power to the PLL phase angle correction and therefore also impacts the angle that the PLL calculates. Which is the entire reason of changes in voltage measurements and hence also active and reactive power. So in summary,

any change in frequency impacts the PLL phase angle correction, not directly the active or reactive power.
In a tool such as PSS®E the bus voltages and angles are calculated based on the network solution within a transient stability solution framework. So, the network side bus voltages and angles are updated every solution, meaning every time step of the dynamic solution when PSS®E calls the network solution. Therefore the changes in bus voltages and angles are instantaneous (based on network solution/algebraic equations) and it does not exist no such thing as d-q transformation of the voltages that will change with respect to a change in the phase angle. As a result of this, if the grid frequency changes it will not directly impact the bus angle calculation and even if that would be the case it is not directly related to active power/DC-voltage of a converter. On the other hand, in a dynamic model such as a synchronous generator in PSS®E, frequency/speed and angle deviations $\Delta\omega$ and $\Delta\delta$ respectively are modeled as swing equations as a part of the machines differential equations which are linked to turbine and governor model that regulates the active power. So there is a direct link between active power and change in frequency or speed. In a user defined E-STATCOM model these links needs to be established and is part of a future work. One way to establish this link is to write a user defined PLL model (which has been already implemented), but the challenge is how to interface the calculated phase angle correction of the PLL to the network solution where the actual bus voltage magnitude and angle is updated. PSS®E does not allow the user to access the network solution arrays within the dynamic solution. Alternative approaches needs to be looked into in more detail and may be out of scope of this project. Therefore it is kept as a future work.

5.4 Discussion on Comparison to VMPSCAD

As mentioned previously the network that is used to test the E-STATCOM in VMPSCAD is different than that of the PSS®E, where in VMPSCAD the network consists of two E-STATCOMs that shares the load between each other. This will make a direct comparison not possible, but the general behavior of the signals can be discussed and compared. The behavior of the active power output from the E-STATCOM in the PSS®E-model and VMPSCAD-model is similar as seen in the lower graph of Figure 4.15. The only difference between the two models is that the PSS®E-model stabilizes at 0 pu faster. The reason for why the PSS®E-model's output power jumps to -20 MW instantly is because the the current I_{d_final} from (3.17) is equal to 0 pu when the first calculation of the output equation (3.19) is made. The program will therefore, as default, output a current and an active power $POUT$ shown in 4.15 that balances the load changes immediately. Since the load change signal is a square-wave the default output of active power will be a square-wave as well. When the next iteration is calculated I_{d_final} will have a value not equal to 0 pu and that value will be subtracted from the first iteration. The calculation of (3.19) will continue and for every iteration the new value of I_{d_final} will be subtracted from the previous value of the output current. That is why the behavior of $POUT$ and I_d in Figure 4.14 is similar apart from the initial decrease that comes from the default

behavior of PSS®E-model when I_{d_final} is equal to 0 pu.

The upper graph which shows the frequency of the two models shows that the VMPSCAD-model keeps the frequency close to 50 Hz while the PSS®E-model has a frequency drop during the load change and after the frequency does not come back to 50 Hz. This indicates that the PSS®E-model, even though it has a similar output as the VMPSCAD-model during the same load change, does not regulate the frequency as it should. It is expected that the E-STATCOM should act on the load change, which it does, and begin to generate or absorb active power in order to keep the frequency at 50 Hz. Why it fail to do so might be because the two programs models differ. The same output may give different results even though the behavior of the disturbance in the system is the same. But the fact that the PSS®E-model does not even manage to come back to 50 Hz after the load change indicates that there is some parameter that does not go back to its initial value. The problem is that when the output power has stabilized at 0 after the load is applied the frequency continues to decrease, which can be seen in Figure 4.3 and 4.7. Because it keeps decreasing the frequency value at 2 seconds will not be equal to the value when the output becomes 0 pu at 1.5 seconds. The decrease over time combined with the small frequency drop after the load is removed results in a frequency not equal to 50 Hz. The problem with the decreasing frequency when the load is applied is also present after the load is removed. Even though the output from the E-STATCOM is 0 MW and the load is removed the frequency drops which shows that some parameter the frequency depends on continue to change.

5.5 Under voltage

The fault is tested on the system to show that the original effect of the STATCOM, to support reactive power during voltage disturbances on the system still works as intended. The fault that is applied is an inductive fault of 0.064 H during 0.1 seconds to simulate an under voltage. The response of the d- and q-components can be seen in Figure 4.16 where there are some oscillations on i_d (upper graph) when the fault is applied and removed but otherwise it stays constant at zero, which is expected since no active power support is needed. i_q also has some oscillations when the fault is applied but stabilizes at around 1.3 pu during the time the fault is applied in order to support with reactive power. It then decreases towards zero when the fault is removed since there now is no need for reactive power support. The oscillations that occur here for both i_d and i_q is in its magnitude large but they transfer over to a constant value quick. The size of these oscillations could be made smaller if more time was put in to fine tuning the virtual impedance parameters, but since the focus on this project was the active power support from the E-STATCOM the parameters were tuned according to those disturbances. The fault is just presented in order to show that the reactive power support of the system still works as intended.

The AC-voltage on bus SVS HV and the reactive power output of the E-STATCOM can be seen in 4.17. Where the AC-voltage (upper graph) can be seen dropping when the fault is applied at 0.5 seconds and then stay constant due to the support from the reactive power, which can be seen oscillating when the fault is applied and

then providing a constant reactive power to support the voltage during the fault. When the fault is removed there are some oscillations on the AC-voltage before it fully recovers back to its initial value of 1 pu, the same goes for the reactive power output but the oscillations are larger which is due to the same reason as for the current components. But as mentioned the main reason for presenting this was to show that the E-STATCOM still is able to provide reactive power support and bring back the voltage to its initial value after a fault on the system.

5.6 Ethics

As a modern engineer it is important to understand and consider the ethical questions and impacts a thesis/project can have on our society. This chapter will discuss the societal, ethical and ecological impact from this thesis.

5.6.1 Societal impact

In 2015 the UN set up 17 sustainable development goals that are to be achieved by 2030 in order to create a better world than the one we live in today [22]. Two of the 17 goals that this thesis can contribute to are goal 7 'Affordable and clean energy' and goal 13 'Climate action'. With goal 7, the UN want renewable energy sources to become cheaper, more reliable and more efficient which would lead to a world that is less dependent on conventional energy source. A world that is not dependent on conventional energy sources is a world with less carbon dioxide emissions.

E-STATCOM with GFM and its ability to control the active and reactive power flow in the transmission system can be a part of the strive to reach a reliable and stable power grid. Now when the world is focusing more on building renewable power sources it can cause some problem for the power grids inertia. While the conventional energy sources are running on the technology of synchronous generators that support the grid with inertia, renewable energy sources usually does not. To solve this problem the renewable energy sources needs to be able to support the grid with the inertia necessary to keep the frequency stable. One method for this solution is to control the power electronics that renewable sources are based on to act as a synchronous generator and by doing so trick the power grid into thinking that it is a synchronous generator. This is what GFM does and why GFM can be a important tool when our society is changing into a world with a stable and effective power grid that is based on renewable energy sources.

Making this method common practice would allow for developing countries to create a stable electricity infrastructure based on their available renewable energy sources. This would allow these countries to in a higher pace develop their economic infrastructure and their technical development. This will allow for a lot of possibilities such as more job opportunities, better opportunities and environments for studying, being inline with UN goals 4 (Quality Education) and 8 (Decent work and Economic growth).

5.6.2 Ethical impact

An example of an ethical question is if it is okay to let developing countries slow down the process of reducing carbon dioxide emissions in order to build more industries and evolve as a country. This thesis could help speed up the developing countries industrial revolution without putting as much stress on the environment, with the use of renewable energy sources and a stable electricity infrastructure instead of the use of conventional energy sources.

When it comes to the writing of the thesis there are some ethical aspects that also has to be considered. It is important that the references are done in a proper way so that the credit is given to the author(s) of the source. If the reference is wrong or if some text is copied from another report this report will be classed as plagiarised, which breaks against an important ethical rule in academia.

5.6.3 Ecological impact

The implementation of GFM to further develop the applications and possibilities of renewable energy sources and to create a power grid that is not depending on conventional energy will have some ecological impacts that has to be discussed. A newly built wind power plant for example can be troublesome for birds that live in or close to that area. Birds can die when colliding with the rotor blades, this is especially common for birds of prey since they usually hunt for food on the ground which means that their vision is focused downwards [23].

When wind power farms are being built off-shore it can disturb the fishes that lives there. However off-shore wind farms can have some good effects on the ecosystem in the water as well. There are rules in some countries that makes it illegal to fish around off-shore wind farms [24]. This creates a safe playground/haven for the fishes which can benefit the wildlife.

6
Conclusion

The model of the E-STATCOM that is built in PSS®E responds to a change in active power on the network, by decreasing the RoCoF and stabilizing the frequency during the time the load is connected and almost moving it back to its initial value when the load is disconnected. The behavior of the active power output from the E-STATCOM in PSS®E during a load change is similar to the behavior in VMPSCAD during the same load change. However it is not able to move the frequency back to its initial value during the time the load is connected. It does not respond to only a frequency change in the system. The major reason why this is happening is due to the fact that the system responds to an active power change and not to a frequency change, therefore it is not able to respond to only a frequency change either. An alternative approach where the active power is calculated based on the frequency deviation was introduced and showed good potential on its initial response, however further development has to be done regarding this approach. Due to the fact that it can only keep the system stable for a short duration before it crashes. However the equations that are used to form the different control parts of the model should also work for the suggested solution, since they respond as intended for the tested cases. They only need some small changes in order for them to fit with the new calculated active power. Another reason on why the system does not respond to a frequency change is due to how PSS®E operates, where the phase angle cannot be updated by the user. Which then will not allow for the E-STATCOM to see a change in frequency. A possible solution to this would be to somehow be able to update the phase angles of the bus voltages with the PLL phase angle correction, allowing for the system to respond.

So even if the final product of this project does not behave fully as intended, the missing parts to make it work as intended has been located and a possible solution has been suggested.

6.1 Future work

In this section follows suggestions on how the project can continue

- Look into how to fully implement the frequency dependent active power.
- Fix so that the PSC-angle goes back to zero after disturbance.
- Further develop the PLL in detailed manner, so that frequency changes impacts voltage measurements.
- Test in different networks to verify its behavior.

References

[1] R. H. Lasseter, Z. Chen, and D. Pattabiraman, "Grid-forming inverters: A critical asset for the power grid," *IEEE Journal of Emerging and Selected Topics in Power Electronics*, vol. 8, no. 2, pp. 925–935, 2020. DOI: 10.1109/JESTPE.2019.2959271.

[2] D. Pattabiraman, R. H. Lasseter., and T. M. Jahns, "Comparison of grid following and grid forming control for a high inverter penetration power system," in *2018 IEEE Power Energy Society General Meeting (PESGM)*, 2018, pp. 1–5. DOI: 10.1109/PESGM.2018.8586162.

[3] D.-P. Sadik, "On reliability of sic power devices in power electronics," Ph.D. dissertation, Kungl Tekniska högskolan, May 2017.

[4] N. G. Hingorani and L. Gyugyi, *Understanding FACTS: Concepts and technology of flexible AC transmission systems*. IEEE Press, 2000, ISBN: 0-7803-3455-8.

[5] N. Mohan, T. M. Undeland, and W. P. Robbins, *Power Electronics*. John Wiley & Sons, Inc., 1995, ISBN: 0-471-58408-8.

[6] M. Works, *Gto-based statcom*, https://se.mathworks.com/help/physmod/sps/powersys/ug/gto-based-statcom.html, Accessed: 2022-03-21, 2022.

[7] L. Zhang, X. Hu, Z. Wang, F. Sun, and D. G. Dorrell, "A review of supercapacitor modeling, estimation, and applications: A control/management perspective," *Renewable and Sustainable Energy Reviews*, vol. 81, pp. 1868–1878, 2018, ISSN: 1364-0321. DOI: https://doi.org/10.1016/j.rser.2017.05.283. [Online]. Available: https://www.sciencedirect.com/science/article/pii/S1364032117309292.

[8] A. Yu, V. Chabot, and J. Zhang, *Electrochemical Supercapacitors For Energy Storage and Delivery: Fundamentals And Applications*. CRC Press and Taylor & Francis Group, 2013, ISBN: 978-1-4398-6989-5.

[9] A. González, E. Goikolea, J. A. Barrena, and R. Mysyk, "Review on supercapacitors: Technologies and materials," *Renewable and Sustainable Energy Reviews*, vol. 58, pp. 1189–1206, 2016, ISSN: 1364-0321. DOI: https://doi.org/10.1016/j.rser.2015.12.249. [Online]. Available: https://www.sciencedirect.com/science/article/pii/S1364032115016329.

[10] U. of Cambridge, *The electrical double layer*, https://www.ceb.cam.ac.uk/research/groups/rg-eme/Edu/the-electrical-double-layer, Accessed: 2022-03-21, 2022.

[11] Y. Yang, Y. Han, W. Jiang, *et al.*, "Application of the supercapacitor for energy storage in china: Role and strategy," *Applied Sciences*, vol. 12, no. 1, p. 354, 2021.

[12] P. P. Barker, "Ultracapacitors for use in power quality and distributed resource applications," in *IEEE Power Engineering Society Summer Meeting,*, IEEE, vol. 1, 2002, pp. 316–320.

[13] P. Tielens and D. Van Hertem, "The relevance of inertia in power systems," *Renewable and Sustainable Energy Reviews*, vol. 55, pp. 999–1009, 2016, ISSN: 1364-0321. DOI: https://doi.org/10.1016/j.rser.2015.11.016.

[14] B. Lennartsson, *The TEX Book*. Addison-Wesley Professional, 1986.

[15] W. J. Praiselin and J. B. Edward, "3 - integrated renewable energy sources with droop control techniques-based microgrid operation," in *Hybrid-Renewable Energy Systems in Microgrids*, ser. Woodhead Publishing Series in Energy, A. H. Fathima, N. Prabaharan, K. Palanisamy, *et al.*, Eds., Woodhead Publishing, 2018, pp. 39–60, ISBN: 978-0-08-102493-5. DOI: https://doi.org/10.1016/B978-0-08-102493-5.00003-0. [Online]. Available: https://www.sciencedirect.com/science/article/pii/B9780081024935000030.

[16] R. Moslemi, J. Mohammadpour, and A. Mesbahi, "A modified droop control for reactive power sharing in large microgrids with meshed topology," in *2016 American Control Conference (ACC)*, 2016, pp. 6779–6784. DOI: 10.1109/ACC.2016.7526739.

[17] S. Energy, *Most efficient way of controlling reactive power*, https://www.siemens-energy.com/global/en/offerings/power-transmission/portfolio/flexible-ac-transmission-systems/msc-mscdn.html, Accessed: 2022-04-01, 2022.

[18] G. Li, F. Ma, A. Luo, *et al.*, "Virtual impedance-based virtual synchronous generator control for grid-connected inverter under the weak grid situations," *IET Power Electronics*, vol. 11, no. 13, pp. 2125–2132, 2018. DOI: 10.1049/iet-pel.2018.5200.

[19] A. Adib and B. Mirafzal, "Virtual inductance for stable operation of grid-interactive voltage source inverters," *IEEE Transactions on Industrial Electronics*, vol. 66, no. 8, pp. 6002–6011, 2019. DOI: 10.1109/TIE.2018.2874594.

[20] L. Zhang, L. Harnefors, and H.-P. Nee, "Power-synchronization control of grid-connected voltage-source converters," *IEEE Transactions on Power Systems*, vol. 25, no. 2, pp. 809–820, 2010. DOI: 10.1109/TPWRS.2009.2032231.

[21] *Powerfactory 2021*, Sep. 2021. [Online]. Available: https://www.digsilent.de/en/newsreader/digsilent-releases-powerfactory-2021-sp5.html.

[22] UN, *The global goals*, https://www.globalgoals.org/, Accessed: 2022-01-26, 2022.

[23] Naturvårdsverket, *Vindkraftens påverkan på fåglar och fladdermöss*, https://www.naturvardsverket.se/om-miljoarbetet/forskning/vindval/vindkraftens-paverkan-pa-faglar-och-fladdermoss/, Accessed: 2022-02-03.

[24] MSP, *Offshore wind and fisheries*, https://maritime-spatial-planning.ec.europa.eu/sector-information/offshore-wind-and-fisheries, Accessed: 2022-02-03, 2021.

A

Appendix 1

A.1 Electric Double Layer

Figures of how the theory regarding electric double layer developed from Helmholtz idea to Gouy & Chapman and Stern & Grahame. The molecules with no sign on them in the figures represent solvent. Depending on surrounding parameters the diffuse layer, seen in Figure A.2, can be really thin so that the distance between the ions is the size of solvent such as water in a aqueous solution, which is the Helmholtz layer in Figure A.1. Later Stern and Grahame showed that these two layers coexist as in the Stern-Grahame model shown in Figure A.3.

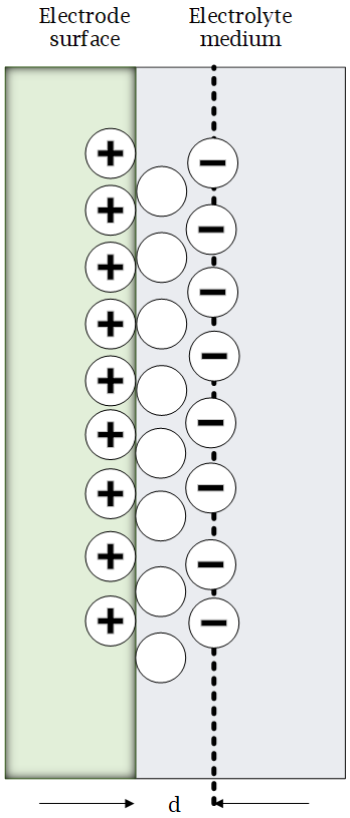

Figure A.1: Helmholtz layer.

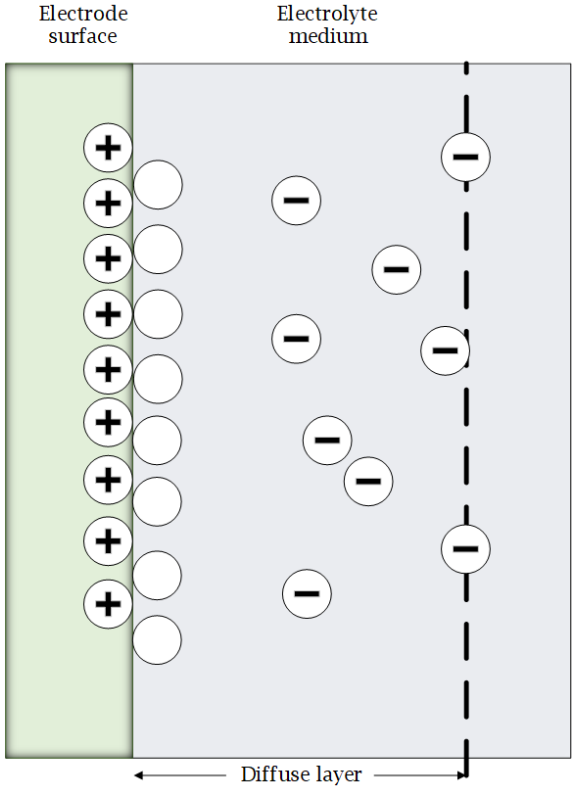

Figure A.2: Diffuse-layer between electrode and electrolyte

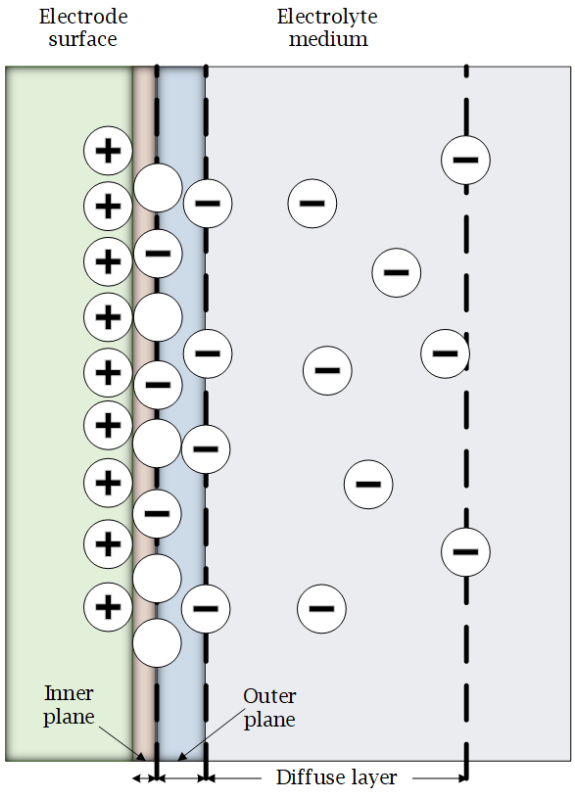

Figure A.3: Stern-Grahame model where the red area is the inner plane and the blue area is the outer plane.

A.2 Simulation network

Network used in PSS®E to test behavior and response from E-STATCOM when subjected to different cases.

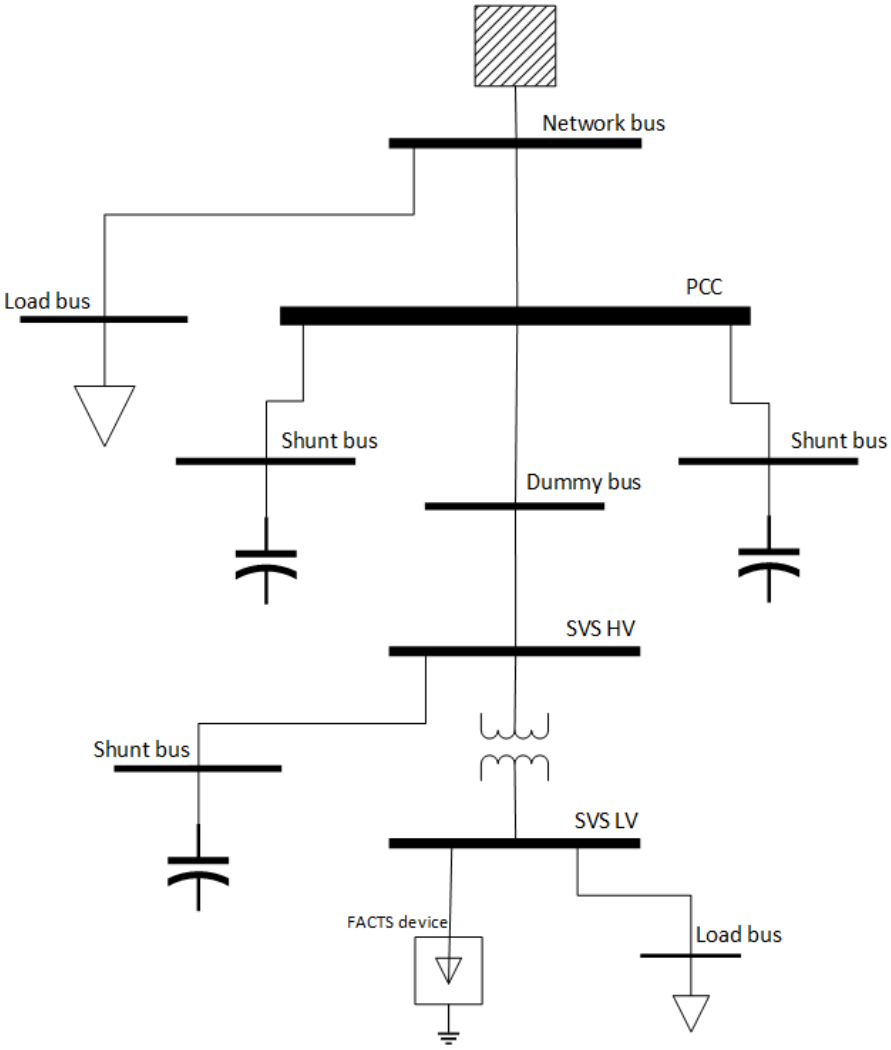

Figure A.4: System used for tests on the E-STATCOM

DEPARTMENT OF ELECTRICAL ENGINEERING
CHALMERS UNIVERSITY OF TECHNOLOGY
Gothenburg, Sweden
www.chalmers.se

CHALMERS
UNIVERSITY OF TECHNOLOGY